



Published in final edited form as:

Cell Rep. 2022 September 27; 40(13): 111402. doi:10.1016/j.celrep.2022.111402.

## Ventral hippocampus-lateral septum circuitry promotes foraging-related memory

Léa Décarie-Spain<sup>1,5</sup>, Clarissa M. Liu<sup>1,2,5</sup>, Logan Tierno Lauer<sup>1</sup>, Keshav Subramanian<sup>1,2</sup>, Alexander G. Bashaw<sup>1,2</sup>, Molly E. Klug<sup>1</sup>, Isabella H. Gianatiempo<sup>1</sup>, Andrea N. Suarez<sup>1</sup>, Emily E. Noble<sup>4</sup>, Kristen N. Donohue<sup>1</sup>, Alyssa M. Cortella<sup>1</sup>, Joel D. Hahn<sup>3</sup>, Elizabeth A. Davis<sup>1</sup>, Scott E. Kanoski<sup>1,2,6,\*</sup>

<sup>1</sup>Human and Evolutionary Biology Section, Department of Biological Sciences, Dornsife College of Letters, Arts and Sciences, University of Southern California, 3616 Trousdale Pkwy, Los Angeles, CA 90089, USA

<sup>2</sup>Neuroscience Graduate Program, University of Southern California, 3641 Watt Way, Los Angeles, CA 90089, USA

<sup>3</sup>Neurobiology Section, Department of Biological Sciences, Dornsife College of Letters, Arts and Sciences, University of Southern California, 3616 Trousdale Pkwy, Los Angeles, CA 90089, USA

<sup>4</sup>Department of Foods and Nutrition, University of Georgia, 305 Sanford Drive, Athens, GA 30602, USA

<sup>5</sup>These authors contributed equally

<sup>6</sup>Lead contact

### SUMMARY

Remembering the location of a food or water source is essential for survival. Here, we reveal that spatial memory for food location is reflected in ventral hippocampus (HPCv) neuron activity and is impaired by HPCv lesion. HPCv mediation of foraging-related memory involves communication to the lateral septum (LS), as either reversible or chronic disconnection of HPCv-to-LS signaling impairs spatial memory retention for food or water location. This neural pathway selectively encodes appetitive spatial memory, as HPCv-LS disconnection does not affect spatial memory for escape location in a negative reinforcement procedure, food intake, or social and olfactory-based appetitive learning. Neural pathway tracing and functional mapping analyses reveal that LS neurons recruited during the appetitive spatial memory procedure are primarily

This is an open access article under the CC BY-NC-ND license (<http://creativecommons.org/licenses/by-nc-nd/4.0/>).

\*Correspondence: kanoski@usc.edu.

#### AUTHOR CONTRIBUTIONS

L.D.-S., C.M.L., E.A.D., and S.E.K. conceived and performed experiments and wrote the manuscript. L.T.L., K.S., A.G.B., M.E.K., I.H.G., A.N.S., K.N.D., and A.M.C. performed experiments. E.E.N. provided expertise. J.D.H. performed experiments and provided expertise.

#### SUPPLEMENTAL INFORMATION

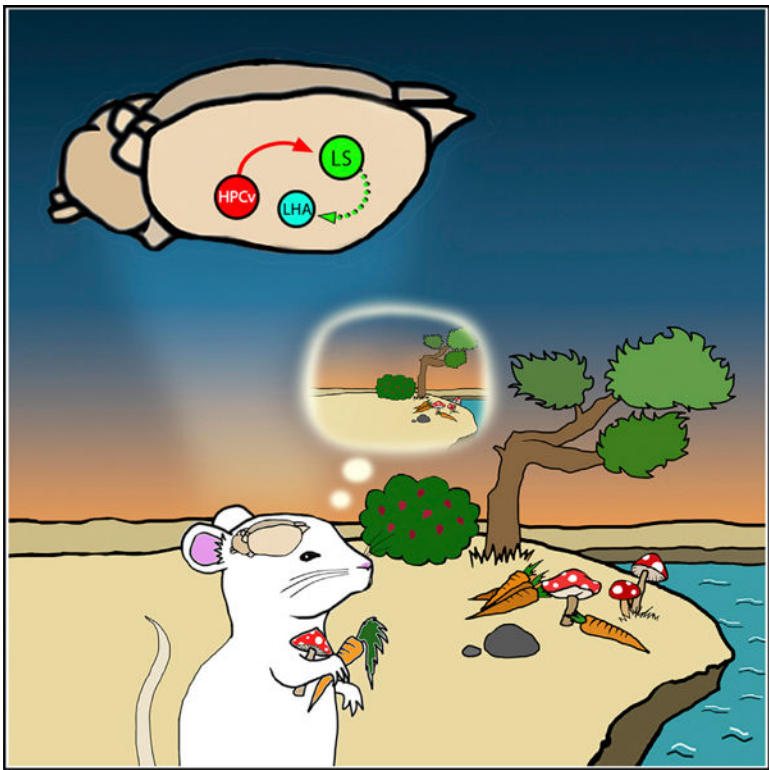
Supplemental information can be found online at <https://doi.org/10.1016/j.celrep.2022.111402>.

#### DECLARATION OF INTERESTS

The authors declare no competing interests.

GABAergic neurons that project to the lateral hypothalamus. Collective results emphasize that the neural substrates controlling spatial memory are outcome specific based on reinforcer modality.

**Graphical abstract**



**In brief**

How do hungry or thirsty animals find food or water? Décarie-Spain et al. identify a ventral hippocampus to lateral septum circuit that selectively promotes spatial memory for appetitive-based (food or water) but not aversive-based (escape) reinforcement. These findings identify a neural pathway that selectively encodes foraging-related memory.

**INTRODUCTION**

A survival advantage common to early humans and lower-order mammals is the ability to accurately remember the location of a food or water source in the environment and efficiently navigate back to a shelter or other safe location. The neurobiological substrates that regulate visuospatial navigation are therefore critical to effectively implement food-directed or water-directed foraging behavior. In rodents, a number of maze tasks have been developed that have been instrumental in identifying brain structures within the telencephalon that are essential for visuospatial mapping and egocentric orientation in the environment, including the hippocampus and the medial entorhinal cortex, respectively (Morris, 1997; Rowland et al., 2016). However, despite reliably locating food and water sources in the environment being a key selection pressure driving the evolution of

visuospatial navigation, the overwhelming majority of rodent model research on the neural substrates of spatial learning and memory have utilized procedures such as the Morris water maze and the Barnes maze that each involve escaping aversive stimulus conditions (Barnes, 1979; Morris, 1984). Furthermore, while single-unit recordings have been used to identify specific populations of neurons that subserve distinct navigational functions (e.g., hippocampal “place cells,” medial entorhinal “grid cells”) (Hafting et al., 2005; O’Keefe and Dostrovsky, 1971), and these neurons have been shown to respond to taste (Herzog et al., 2019, 2020; Ho et al., 2011), the bulk of this research has recorded neural activity under neutral conditions devoid of either appetitive or aversive reinforcement. Very little research has been dedicated to identifying brain regions and neural circuits that may specifically promote spatial memory based on the location of appetitive reinforcers (e.g., food, water), as well as the extent to which the nature of the reinforcement is a critical factor in deciphering the brain’s control of visuospatial navigation.

Rodent model research investigating brain regions that mediate visuospatial navigational memory has predominantly focused on the anterior and “dorsal” subregion of the hippocampus (septal pole; HPCd). However, the posterior and “ventral” hippocampus subregion (temporal pole; HPCv), while classically associated with stress- and affect-associated memory processes (Fanselow and Dong, 2010), also plays a role in visuospatial learning and memory (de Hoz et al., 2003; Keinath et al., 2014; Kjelstrup et al., 2008). For example, under some testing conditions, selective HPCv lesions impair spatial memory performance in the Morris water maze (Ferbinteanu et al., 2003; de Hoz et al., 2003). Moreover, place cells that are responsive to location changes in the visuospatial environment are present within both the HPCd and HPCv pyramidal layers, with a linear increase in the spatial scale of representation from the dorsal to the ventral pole (Kjelstrup et al., 2008). Despite a common role for the HPCd and HPCv in mediating spatial memory, there is also evidence for a functional distinction between the subregions (Fanselow and Dong, 2010; Kanoski and Grill, 2017; Moser and Moser, 1998). For instance, lesions of the HPCv but not the HPCd alter stress responses (Henke, 1990) and anxiety-like behavior (Kjelstrup et al., 2002), whereas HPCd but not HPCv lesions impair spatial memory in an incidental (nonreinforced) procedure (Gaskin et al., 2009). These two HPC subregions also have disparate neuroanatomical connectivity, supporting a framework for a functional diversity in which the HPCd preferentially processes cortical-derived sensory information and the HPCv preferentially processes metabolic and limbic-derived affective information (Fanselow and Dong, 2010; Kanoski and Grill, 2017). These functional distinctions are further supported by the generation of the hippocampus gene expression atlas, which provides a comprehensive integration of gene expression and connectivity across the HPC septotemporal axis (Bienkowski et al., 2018; Gergues et al., 2020). Given that both the HPCv and the HPCd participate in spatial memory but have distinct neuroanatomical connectivity and contributions when it comes to regulating other cognitive and mnemonic processes, it is feasible that the HPCv and HPCd support different forms of spatial memory depending on the type of reinforcement and/or the context associated with the behavior.

Recent findings identify the HPCv as a critical brain substrate in regulating feeding behavior and food-directed memory processes. Reversible inactivation of HPCv neurons after a meal increases the size of and reduces the latency to consume a subsequent meal (Hannapel et

al., 2017, 2019). In addition, receptors for feeding-related hormones are more abundantly expressed in the HPCv compared with the HPCd (e.g., ghrelin receptors [Mani et al., 2014; Zigman et al., 2006], glucagon-like peptide-1 [GLP-1] receptors [Merchenthaler et al., 1999]), and these HPCv endocrine and neuropeptide receptor systems alter food intake and feeding-related memory (Hsu et al., 2015a, 2018b, 2018a; Kanoski et al., 2011, 2013; Suarez et al., 2020). Olfactory information, which is intimately connected with feeding behavior, is also preferentially processed within the HPCv rather than the HPCd (Aqrabawi and Kim, 2018; Aqrabawi et al., 2016). The HPCv field CA1 (CA1v), specifically, is bidirectionally connected to brain regions that process olfactory information (Fanselow and Dong, 2010; De La Rosa-Prieto et al., 2009; Petrovich et al., 2001), and CA1v neurons respond more robustly to olfactory contextual cues than CA1d neurons (Keinath et al., 2014). Given these appetite-relevant HPCv neuroanatomical connections, endocrine and neuropeptide receptor expression profiles, and functional evidence linking this subregion with food-motivated behaviors, we hypothesize that HPCv mediation of visuospatial memory is preferentially biased to appetitive food- and water-reinforced foraging behavior.

HPCv pyramidal neurons have extensive projection targets throughout the brain (Swanson and Cowan, 1977), yet the functional relevance of these pathways is poorly understood. The lateral septum (LS) is a robust target of HPCv glutamatergic pyramidal neurons (Arszovszki et al., 2014; Risold and Swanson, 1996). Given that this pathway has been shown to affect feeding behavior (Kosugi et al., 2021; Sweeney and Yang, 2015) and that neuroplastic changes occur in the LS after learning a spatial memory task (Garcia et al., 1993; Jaffard et al., 1996), we predict that HPCv-to-LS projections participate in regulating foraging-related spatial memory for food and water location. To investigate this hypothesis, we developed two appetitive reinforcement-based spatial foraging behavioral tasks that allow for direct comparison with an aversive reinforcement-based task of similar difficulty that uses the same apparatus and spatial cues. First, foraging-related spatial memory was assessed following neurotoxic ablation of the HPCv, and CA1v bulk intracellular calcium activity was recorded during memory probe performance in intact control animals. Performance in these tasks was next assessed following pathway-specific dual viral-based reversible (chemogenetic inhibition) or chronic (targeted apoptosis) disconnection of the CA1v-to-LS pathway. To further expand neural network knowledge on CA1v-to-LS signaling, we used conditional viral-based neuroanatomical tracing strategies to identify both first-order collateral and second-order targets of LS-projecting CA1v neurons, as well as immediate-early gene mapping approaches to confirm the functional relevance of downstream pathways. Collective results from the present study identify a neural circuitry of specific relevance to foraging behavior.

## RESULTS

### Ventral hippocampus neurons encode memory for the spatial location of food

To examine the importance of the HPCv in memory for the spatial location of food reinforcement, HPCv bulk calcium-dependent activity was recorded in animals performing a food-reinforced appetitive visuospatial memory task that utilizes a Barnes maze apparatus (Figure 1A). Fiber photometry recordings in the HPCv (representative injection site in

Figures 1B and 1C) revealed HPCv activity fluctuations in response to escape hole investigations during the appetitive visuospatial memory task memory probe in which no food was present (Figure 1D; time  $\times$  investigation type,  $p < 0.05$ ). HPCv changes in neuron activity immediately following escape hole investigation differ between investigation type (correct versus incorrect, Figure 1E;  $p < 0.05$ , Cohen's  $d = -1.0582$ ), such that 5-s calcium activity increased following correct hole investigations yet decreased following incorrect hole investigations. In addition, a significant correlation was found between changes in HPCv activity 5 s following a hole investigation and distance from the appropriate escape hole (Figure 1F;  $p < 0.01$ ,  $r^2 = 0.08584$ ). To verify whether the HPCv is necessary for food location-based spatial memory, another group of animals received bilateral *N*-methyl-D-aspartate excitotoxic lesions of the HPCv or bilateral sham injections (histological analyses for the neuron-specific NeuN antigen in Figure 1G) and were tested with the appetitive visuospatial memory task (representative behavioral traces in Figure 1H). Results revealed no significant differences in errors (incorrect hole investigations) (Figure 1I) or latency to locate the food source hole (Figure 1J) during training. However, memory probe results show that animals with HPCv lesions decreased the ratio of correct + adjacent/total holes explored compared with controls (Figure 1K; control versus HPCv lesion,  $p < 0.05$ , Cohen's  $d = -1.0174$ , *t* test; control group different from chance performance,  $p < 0.001$ , one-sample *t* test), indicating impaired memory for the spatial location of food reinforcement.

Postsurgical analyses of food intake (Figure S1A) and body weight (Figure S1B) found no significant group differences in these measures over time. These collective results indicate that the HPCv is required for memory retention but not learning of the spatial location of food in the environment, and that HPCv neural activity is modulated by appetitive spatial memory accuracy.

### **Ventral hippocampus CA1 projections to the lateral septum mediate appetitive spatial memory for food or water location, but not aversive spatial memory for escape location**

To identify a specific neural pathway mediating the results described above, we investigated the functional relevance of the CA1v-to-LS signaling in learning and recalling the spatial location of either food or water reinforcement using conditional dual viral approaches to either reversibly (via Cre-dependent pathway-specific inhibitory chemogenetics with clozapine-N-oxide [CNO] administration prior to the memory probe; diagram of approach in Figure 2A) or permanently (via Cre-dependent pathway-specific caspase-induced lesions; diagram of approach in Figure 2B) disconnect CA1v-to-LS communication. Results from the appetitive food-seeking spatial memory task reveal no significant group differences during training in either errors before locating the correct hole (Figure 2D) or latency to locate the food source hole (Figure 2E). However, memory probe results demonstrate that both acute (pathway-specific designer receptors exclusively activated by designer drugs [DREADDs]) and chronic (pathway-specific caspase) CA1v-to-LS disconnection decreased the ratio of correct + adjacent/total holes explored compared with controls (Figure 2F; control versus DREADDs and control versus caspase,  $p < 0.05$ , Cohen's  $d = -1.142$ ; control different from chance,  $p < 0.0001$ , caspase different from chance,  $p < 0.05$ , one-sample *t* test), indicating impaired memory for the spatial location of food reinforcement.

Results from an analogous appetitive water-seeking spatial memory task in a separate cohort of water-restricted rats also reveal no significant group differences during training in either errors before locating the correct hole (Figure 2G) or latency to locate the water source hole (Figure 2H). However, a significant impairment was observed following either acute or chronic CA1v-to-LS disconnection of the ratio of correct + adjacent/total holes explored compared with controls (Figure 2I; control versus DREADDs and control versus caspase,  $p < 0.05$ , Cohen's  $d = -1.18$ ; control different from chance,  $p < 0.01$ , DREADDs and caspase different from chance,  $p < 0.05$ , one-sample  $t$  test), indicating impaired memory for the spatial location of water reinforcement.

Histological analyses confirmed successful viral transfection of LS-projecting CA1v neurons with DREADDs (Figure 2C), as well as successful lesioning of LS-projecting CA1v neurons for the caspase approach (Figures S2G and S2H). The reversible DREADDs-based disconnection approach was further confirmed by c-Fos analyses in the LS, where the number of c-Fos immunoreactive neurons in the LS in response to the food reinforcement-based spatial memory probe test was reduced following CNO treatment relative to vehicle/control treatment (Figures S2A–S2C;  $p < 0.01$ , Cohen's  $d = -3.9578$ ). We further confirmed that intracerebroventricular (i.c.v.) administration of CNO failed to influence LS neuronal activation in the absence of inhibitory DREADDs (Figures S2D–S2F). Postsurgical analyses of food intake (Figure S1C) and body weight (Figure S1D) found no group differences in these measures over time (in the absence of CNO treatment). These data demonstrate that the CA1v-LS disconnection approaches were successful, that CA1v-to-LS communication is critical for remembering the spatial location of food and water, and that these effects are unlikely to be based on differences in energy status or food motivation.

To evaluate whether CA1v-to-LS signaling is specifically involved in appetitive reinforcement-based spatial memory (food or water) versus spatial memory in general, in a separate cohort of animals we tested the effect of reversible and chronic CA1v-to-LS disconnection in a spatial learning task based on aversive reinforcement rather than food or water. Importantly, this task uses the same apparatus and visuospatial cues as the spatial location food and water memory tasks described above, but the animals are motivated to locate the tunnel to escape mildly aversive stimuli (bright lights, loud noise) with no food or water reinforcement in the tunnel. Training results revealed no significant group differences in errors before correct hole (Figure 2J) nor latency to locate the escape hole (Figure 2K). During the memory probe test, there were no group differences in the ratio of correct + adjacent/total holes investigated (Figure 2L; control, DREADDs, and caspase different from chance,  $p < 0.01$ , one-sample  $t$  test). Postsurgical analyses of food intake (Figure S1E) and body weight (Figure S1F) found no group differences in these measures over time. These collective findings suggest that CA1v-to-LS signaling specifically mediates spatial memory in a reinforcement-dependent manner, playing a role in appetitive (food or water reinforcement) but not aversive (escape-based) spatial memory.

## **Disconnection of CA1v-to-LS signaling does not influence food intake, food-motivated operant responding, nonspatial HPC-dependent appetitive memory, anxiety-like behavior, or locomotor activity**

While the results above suggest that the impairments in food- or water-based spatial memory were not based on long-term changes in food intake or body weight, these experiments were conducted under conditions of either chronic food or water restriction. To examine the role of CA1v-to-LS signaling on feeding behavior under free-feeding conditions, we examined meal pattern feeding analyses in the caspase group versus the control group (chronic CA1v-LS disconnection), and in the DREADDs group following CNO or vehicle (within-subjects design; reversible CA1v-LS disconnection). Results averaged over 5 days revealed no significant effect of chronic CA1v-to-LS disconnection (caspase group) on 24-h meal frequency, meal size, meal duration, or 24-h food intake in comparison with controls (Figures S3A–S3D). Similarly, CNO-induced acute reversible silencing of LS-projecting CA1v neurons (DREADDs group) did not significantly affect 24-h meal frequency, meal size, meal duration, or 24-h food intake relative to vehicle treatment (Figures S3E–S3H). Furthermore, CNO-induced acute disconnection of the CA1v-to-LS pathway had no impact on effort-based lever press responding for sucrose rewards in a progressive ratio reinforcement procedure (Figure S3I). Collectively, these findings show that neither reversible nor chronic CA1v-to-LS disconnection influences food intake under free-feeding conditions nor food motivation in a non-visuospatial task.

The HPCv plays an important role in the social transmission of food preference procedure (STFP) (Carballo-Márquez et al., 2009; Countryman et al., 2005; Hsu et al., 2018a), which tests socially mediated food-related memory based on previous exposure to socially communicated olfactory cues (Figure S4A). However, results revealed that neither chronic nor acute disconnection of CA1v-to-LS signaling affected the STFP preference ratio between groups (Figure S4B), with all three groups performing significantly above chance (based on within-group one-sample t tests,  $p < 0.05$ ).

HPCv-to-LS circuitry has been shown to play a role in mediating anxiety and stress behavior (Parfitt et al., 2017; Trent and Menard, 2010). Given that altered anxiety-like behavior and/or locomotion could produce behavioral changes that may lead to an apparent spatial memory deficit in any of the spatial learning tasks used, we examined whether CA1v-to-LS disconnection yields differences in anxiety-like behavior (zero maze task; Figure S4C) and/or locomotion (open field test). Zero maze results showed no significant group differences in time spent in the open zones (Figure S4D) nor in the number of open zone entries (Figure S4E). In addition, CA1v-to-LS disconnection had no effect on general locomotor activity in the open field test (Figure S4F). These collective results suggest that the observed deficits in food- and water-seeking spatial memory are not secondary to impaired nonspatial appetitive learning, general differences in anxiety-like behavior, or locomotor impairments.

### **Collateral medial prefrontal cortex projections from LS-projecting CA1v neurons do not contribute to appetitive spatial memory**

In addition to the LS, CA1v neurons also robustly project to the medial prefrontal cortex (mPFC), a pathway that we have previously shown to be involved in feeding behavior (Hsu et al., 2018b). To examine whether LS-projecting CA1v neurons have collateral targets in the mPFC or in other brain regions, we utilized a conditional dual viral neural pathway tracing approach that identifies collateral targets of a specific monosynaptic pathway (CA1v → LS; diagram in Figure 3A; representative CA1v and LS injection sites in Figure 3B [left and middle]). Results revealed that LS-projecting CA1v neurons also project to the mPFC (Figure 3B, right), whereas very minimal labeling was observed in other brain regions throughout the neuraxis. Thus, it may be the case that the impaired spatial memory for food location observed following either reversible or chronic CA1v-to-LS disconnection is based, in part, on CA1v-to-mPFC signaling from the same LS-projecting CA1v neurons.

We next sought to test the functional relevance to food-directed spatial memory of a CA1v-originating neural pathway (CA1v to mPFC) that is a collateral target of LS-projecting CA1v neurons. Inhibitory DREADDs were expressed in mPFC-projecting CA1v neurons (diagram of approach in Figure 3C and representative CA1v injection site in Figure 3D), and animals received an i.c.v. infusion of CNO or aCSF 1 h prior to the memory probe. Training results from the appetitive spatial memory task revealed no group differences in errors before locating the correct hole (Figure 3E) or latency to locate the food-baited hole (Figure 3F). Importantly, memory probe results demonstrate that CA1v-to-mPFC disconnection (via CNO treatment) did not alter the ratio of correct + adjacent/total holes explored (Figure 3G; aCSF different from chance,  $p < 0.01$ , CNO different from chance,  $p < 0.001$ , one-sample t test) compared with controls (artificial cerebrospinal fluid [aCSF]). These data collectively demonstrate that CA1v-to-LS mediation of foraging-related memory does not require collateral projections to the mPFC neural pathway and that the impact of i.c.v. CNO administration on memory performance is not generalized to the inhibition of any CA1v projections.

### **Appetitive spatial memory engages LS GABAergic neurons and the lateral hypothalamic area downstream of HPCv-LS signaling**

Fluorescent *in situ* hybridization analyses were used to determine the neurotransmitter phenotype of c-Fos<sup>+</sup> LS neurons that were activated during the appetitive food-seeking spatial memory probe test. Results revealed that ~10% of c-Fos<sup>+</sup> LS neurons express choline acetyltransferase (ChAT, a cholinergic marker; Figure 4A), ~88% of c-Fos<sup>+</sup> LS neurons express GAD1 (a GABAergic marker; Figure 4B), and only ~2% of c-Fos<sup>+</sup> LS neurons express VGlut2 (a glutamatergic marker; Figure 4C). These results suggest that LS neurons engaged during the spatial memory probe are primarily GABAergic (Figure 4D).

A dual viral tracing strategy (diagram of approach in Figure 5A; representative LS injection site in Figure 5B) was utilized to identify downstream targets of LS-projecting CA1v neurons. Results reveal that the lateral hypothalamic area (LHA) is the strongest second-order target of the CA1v-to-LS-projecting neurons (Figures 5C and 5D). Quantitative analyses using a custom-built data-entry platform (Axiome C, created by J.D.H.) are

summarized graphically for a representative animal on a brain flatmap summary diagram (Figure 5D) for the hemisphere ipsilateral and contralateral to the injection sites (see Table S1 for data from complete forebrain analyses). Retrograde transfection of the adeno-associated viruses (AAVs) from the injection sites was not observed, as tdTomato<sup>+</sup> cell bodies were only observed in the LS following complete forebrain histological analyses. Additional confirmation of the LHA as a second-order target was provided via a co-injection (COIN) strategy (Suarez et al., 2018; Thompson and Swanson, 2010). This approach involved injections of a monosynaptic retrograde tracer, FluoroGold (FG), in the LHA (representative injection site in Figure 5E) and injection of a monosynaptic anterograde tracer, AAV1-GFP, in the CA1v (representative injection site in Figure 5F), which resulted in the observance of FG-GFP appositions in approximately  $57.57\% \pm 5.04\%$  of FG cell bodies in the LS, thus further confirming this multisynaptic pathway (Figure 5G).

The functional relevance of this pathway to appetitive spatial memory is provided by immediate-early gene mapping of c-Fos<sup>+</sup> cells in the LHA subregions that are most densely innervated downstream of CA1v-to-LS signaling (juxtadorsomedial and juxtaventromedial regions, LHAjd and LHAjv), with results revealing reduced LHA c-Fos expression following appetitive spatial memory probe testing in animals receiving chemogenetic-mediated CA1v-to-LS disconnection (i.c.v. CNO-injected rats) relative to aCSF-injected controls (Figures 5H–5J;  $p < 0.05$ , Cohen's  $d = 1.8833$ ). In contrast, medial LHA c-Fos expression following the appetitive spatial memory probe did not differ by treatment (i.c.v. CNO versus i.c.v. aCSF) in rats without expression of chemogenetic inhibitory receptors in LS-projecting CA1v neurons (Figure S5), thereby further validating the specificity of CNO actions to the inhibitory DREADDs receptor.

Immunohistochemistry analyses were used to determine whether acute disconnection of the CA1v-LS pathway influences c-Fos expression of cells co-expressing the orexin or melanin-concentrating hormone (MCH) neuropeptides in the medial LHA, each of which is associated with appetite-promoting effects (Barson et al., 2013; Lord et al., 2021). Results revealed that approximately 25% of orexin<sup>+</sup> cells in the medial LHA co-express c-Fos following the appetitive spatial memory probe, and this effect did not differ by aCSF versus CNO treatment (Figure S6). A similar analysis in MCH<sup>+</sup> cells of the medial LHA identified only a marginal proportion of MCH<sup>+</sup> c-Fos<sup>+</sup> neurons (3%, data not shown), so additional analysis was not conducted. These findings suggest that CA1v-to-LS signaling does not engage downstream orexin or MCH LHA signaling in the context of appetitive foraging-related memory.

## DISCUSSION

Memory for the physical location of a food or water source is adaptive for maintaining adequate energy supply for reproduction and survival. However, the neural circuits mediating this complex behavior are not well understood, as research on visuospatial memory has predominantly used tasks with either aversive or neutral/passive reinforcement. Moreover, whether the neural circuitry mediating spatial memory function is divergent based on the nature (e.g., appetitive versus aversive) or modality (e.g., food versus water) of the reinforcement has not been systematically investigated. The present study illustrated the

critical role played by the HPCv in an appetitive spatial memory task for food location using both bulk regional calcium-dependent activity recordings and a lesion approach. A monosynaptic CA1v-to-LS pathway is further identified as a necessary substrate for food- and water-motivated spatial memory. Moreover, the selectivity of the CA1v-to-LS pathway in promoting spatial memory for food and water location is supported by results showing that disconnection of this pathway did not affect performance in an escape-motivated spatial memory task of comparable difficulty conducted with the same apparatus, feeding behavior, anxiety-like behavior, locomotor activity, motivated operant responding for palatable food, or olfactory and social-based appetitive memory. Fluorescent *in situ* hybridization analyses also demonstrate that LS neurons engaged during appetitive spatial memory testing are primarily GABAergic. Viral-based pathway tracing revealed that LS-projecting CA1v neurons also send collateral projections to the mPFC; however, functional disconnection of CA1v-mPFC signaling did not impair spatial memory for food location. Utilization of an anterograde multisynaptic viral tracing approach and quantitative forebrainwide axon mapping analyses revealed that the CA1v-to-LS pathway sends second-order projections to various feeding and reward-relevant neural substrates, particularly the LHA, and immediate-early gene functional mapping analyses confirm that this multisynaptic pathway is relevant for appetitive spatial memory. Collectively, these data establish monosynaptic CA1v-to-LS signaling as an essential pathway for spatial memory-based foraging behavior, and we further identify a neural network of interconnected feeding-relevant substrates that are collateral and/or downstream targets of this pathway.

Historically, the hippocampus has been divided into the dorsal and ventral subregions that have both distinct and overlapping functions, anatomical connections, and genetic and receptor expression profiles (Bienkowski et al., 2018; Fanselow and Dong, 2010; Kanoski and Grill, 2017; Moser and Moser, 1998; Swanson and Cowan, 1977). The HPCd has been predominantly implicated in facilitating spatial memory, whereas the HPCv is linked more with stress responses, affective behavior, and energy balance. However, a recent study found that both the HPCd and HPCv were critical for food reward-directed spatial navigation in an obstacle-rich complex environment (Contreras et al., 2018), and under certain testing conditions spatial learning and memory in an aversive reinforcement-based water maze also require both subregions of the HPC (Lee et al., 2019). Here we expand this literature by identifying a specific HPCv-originating pathway (CA1v → LS) that is selectively involved in spatial memory for the location of appetitive (food or water) reinforcement. These findings suggest that the modality of the reinforcement should be considered when investigating the longitudinally organized processing of spatial information across the dorsal-ventral HPC axis.

While HPCv neurons project to multiple regions throughout the neuraxis, projections to the LS are particularly robust (Risold and Swanson, 1996). The LS has been implicated in food anticipatory/seeking behavior, whereby metabolic activation of the lateral septum peaks immediately before feeding (during food anticipatory activity) in rabbit pups (Olivo et al., 2017) and  $\gamma$ -rhythmic input to the LHA from the LS evokes food approach behavior (Carus-Cadavieco et al., 2017). In addition, the LS can bidirectionally modulate food intake via several feeding-relevant neuropeptides, including glucagon-like peptide-1, ghrelin, and urocortin (Maske et al., 2018; Terrill et al., 2016; Wang and Kotz, 2002).

These feeding-associated results are consistent with the contribution of the CA1v-to-LS pathway in promoting spatial memory in the context of foraging but not in the escape-based version of the visuospatial task. Given that the rats were food restricted or water restricted for the respective food- and water-seeking memory tasks, it is likely that a CA1v-to-LS pathway potentiates visuospatial memory in response to changes in internal state. Moreover, this internal state modulation of CA1v-to-LS control of appetitive behavior is specific to foraging-related memory, as disconnection of the circuit did not influence motivated operant responding for the same reinforcer (sucrose) used in the food-seeking spatial memory task.

Recent findings demonstrate that DREADDs-mediated disconnection of an HPCv-to-LS pathway (from CA3v and ventral dentate gyrus [DGv]) increases food intake in mice, with opposite/hyperphagic effects observed following activation of this pathway (Sweeney and Yang, 2015). Here we observe no differences in food intake or meal parameters following DREADDs-mediated acute silencing of the CA1v-to-LS pathway in rats with unlimited access to food and water, therefore establishing a role for this pathway in foraging-relevant memory processes under conditions that are more relevant to normal mammalian behavior, whereby food and water are not freely available. HPCv projections to the LS have also been shown to influence anxiety-like behaviors (Parfitt et al., 2017; Trent and Menard, 2010). However, neither our acute nor chronic disconnection model of the CA1v-to-LS pathway affected these behaviors. Given that these studies targeted the HPCv either independently of subregion or targeted CA3v and DGv, it is probable that functions of HPCv-to-LS pathways differ according to subregional specificity. In fact, a recent study demonstrated opposite effects of inhibition of CA1v and CA3v projections to the LS on approach-avoidance conflict resolution (Yeates et al., 2022).

This work focused on the contribution of an HPCv-to-LS neural pathway to foraging-related memory, yet it is likely that the HPCd also partakes in appetitive spatial memory. In fact, lesions of the HPCd were reported to impair performance in a reinforced radial arm maze procedure (Gaskin et al., 2009), and simultaneous recordings from HPCd and LS cells revealed comparable activity patterns in these two regions during spatial navigation toward a food reward (Wirtshafter and Wilson, 2020). Foraging-relevant memory processing in the HPCd may also engage the LS, as oscillatory patterns from HPCd neurons are predictive of interstitial peripheral glucose dynamics via projections to the LS (Tingley et al., 2021). In addition, the feeding-related neuropeptide MCH was shown to promote spatial learning and memory consolidation by strengthening excitatory signaling within an HPCd-to-LS neural pathway (Liu et al., 2022). The extent to which HPCv and HPCd inputs to the LS independently promote foraging-related memory remains to be elucidated.

The use of two different but complementary approaches for neural pathway-specific disconnection allowed us to test at the levels of learning and memory separately. For example, the use of a reversible (DREADDs) disconnection procedure allowed us to evaluate the effect of CA1v-to-LS disconnection during the memory probe only, with circuit intact during training (CNO was not administered at any point during training). In contrast, the chronic (caspase) disconnection procedure was performed before training and therefore could have affected learning if CA1v-to-LS pathways were required for the learning of the task. However, our results showed that CA1v-to-LS disconnection did not impair learning,

but rather only memory retention performance in the probe test conducted days after the end of training. Thus, we can now confirm, based on two complementary levels of analysis, that this pathway is involved in longer-term memory recall but not learning/acquisition, which is consistent with recent evidence demonstrating that complete HPCv lesions impair retrieval (probe performance) but not acquisition (learning) in a Morris water maze (Hauser et al., 2020).

While the use of aversive reinforcement-based spatial memory tasks is predominant in the field, the radial arm maze has also been used to investigate food-motivated spatial memory (Olton, 1987). An advantage of the present food-reinforced Barnes maze apparatus-based approach over the radial arm maze procedure is that we have developed parallel procedures that use the same apparatus and visuospatial cues to examine water- and escape-motivated spatial memory, thus offering an arsenal to assess the selectivity of the circuit based on multiple reinforcement modalities (food versus water versus escape/aversive).

Utilizing dual viral approaches and functional immediate-early gene mapping analyses, our findings confirm that the CA1v-to-LS pathway projects downstream to the LHA. This region was the most robust forebrain downstream target of CA1v-to-LS signaling, and this multisynaptic pathway was corroborated by an additional monosynaptic tracing approach that combined retrograde tracing (FG in LHA) and anterograde tracing (AAV1-GFP in CA1v) to confirm a connection relay in the LS. The identification of the majority of LS neurons receiving input from the CA1v as GABAergic, along with the resulting increase in medial LHA c-Fos expression following acute disconnection of the CA1v-to-LS pathway, suggests that this chemogenetic intervention prevents medial LHA local inhibition of excitatory neurons. This is consistent with previous findings reporting disinhibition of LHA GABAergic neurons by projecting GABAergic neurons in the context of feeding (O'Connor et al., 2015; Sweeney and Yang, 2015).

We have previously found that the CA1v sends direct projections to the LHA to modulate food intake and meal size control by the orexigenic gastric hormone, ghrelin (Hsu et al., 2015b; Suarez et al., 2020). In the present study, we highlight a multisynaptic pathway connecting the CA1v to the medial LHA through the LS to promote foraging-related spatial memory. These findings suggest that the CA1v is functionally connected to the LHA through direct and indirect projections to influence food intake and appetitive spatial memory, respectively. Interestingly, the direct CA1v-LHA pathway was shown to target orexin neurons whereas the current study finds that although medial LHA orexin neurons are engaged during the appetitive spatial memory probe, this activation is not influenced by acute disconnection of the CA1v-LS-LHA indirect pathway. Thus, these parallel pathways may be promoting differential feeding-relevant behaviors through different neuronal populations in the LHA, with the indirect pathway mediating appetitive memory and the direct pathway mediating food consumption.

Collective results identify a CA1v-to-LS pathway involved in food- and water-motivated spatial memory, but not escape-motivated spatial memory. Furthermore, the selectivity of this pathway to appetitive spatial memory is supported by data showing that neither chronic nor reversible disruption of CA1v-to-LS signaling influenced various other behavioral

outcomes, including food intake, anxiety-like behavior, locomotor activity, and nonspatial HPC-dependent appetitive memory. We also systematically characterized collateral (mPFC) and second-order (LHA) projections of this pathway that are not functional, and functional (respectively), for appetitive spatial memory. The present results shed light on the neural systems underlying complex learned and motivated behaviors that require functional connections between cognitive and feeding-relevant substrates.

### Limitations of the study

A limitation of the present study is that we did not evaluate “gain of function” of CA1v-to-LS signaling on appetitive spatial memory. However, we note that such gain-of-function approaches are more commonly utilized with models of memory dysfunction. Thus, an important area for follow-up research is to investigate whether enhanced CA1v-to-LS signaling (e.g., via excitatory pathway-specific DREADDs) can augment memory function in models where foraging-related memory is impaired. Another limitation of the present study is that the contribution of a CA1v-to-LS pathway on appetitive spatial memory was only investigated in the context of reference memory. Future research is needed to determine whether CA1v-to-LS signaling is also involved in spatial working memory based on appetitive and/or aversive reinforcement.

## STAR★METHODS

### RESOURCE AVAILABILITY

**Lead contact**—Further information and requests for resources and reagents should be directed to and will be fulfilled by the lead contact, Scott Kanoski (kanoski@usc.edu).

**Materials availability**—This study did not generate new unique reagents.

#### Data and code availability

- Original data have been deposited at the Open Science Framework Repository and are publicly available as of the date of publication. Accession number is listed in the key resources table.
- Original code has been deposited to the Open Science Framework Repository and are publicly available as of the date of publication. Accession number is listed in the key resources table.
- Any additional information required to reanalyse the data reported in this paper is available from the lead contact upon request.

### EXPERIMENTAL MODEL AND SUBJECT DETAILS

Adult male Sprague-Dawley rats (Envigo, 250–275g on arrival) were individually housed in hanging wire cages with *ad libitum* access (except where noted) to water and chow (LabDiet 5001, LabDiet, St. Louis, MO) on a 12h:12h reverse light/dark cycle. All procedures were approved by the University of Southern California Institute of Animal Care and Use Committee. Sample size for all behavioral and neuroanatomical experiments was based

on the authors' extensive experience with the procedures and statistical power analyses (described below).

## METHOD DETAILS

**Appetitive food seeking spatial memory task**—To test visuospatial learning and memory for food reinforcement, we developed a spatial food seeking task modified from the traditional Barnes maze procedure (Barnes, 1979). Throughout this paradigm, animals were maintained at 85% free-feeding body weight. In contrast to the traditional Barnes maze where an animal uses the spatial cues to escape mildly aversive stimuli in the environment (e.g. bright light and loud sound), this task utilizes food as motivation, such that each hidden tunnel contained five 45mg sucrose pellets (cat. no. F0023, Bio-Serv, Flemington, NJ).

The procedure involves an elevated gray circular platform (diameter: 122cm, height: 140cm) consisting of 18 uniform holes (9.5cm diameter) spaced every twenty degrees around the outside edge. Under one of the holes is a hidden tunnel (38.73cm L x 11.43cm W x 7.62cm D and a 5.08cm step). Surrounding the table are distinct spatial cues on the wall (e.g., holiday lights, colorful shapes, stuffed unicorn) that are readily visible to the animal. Additionally, a quiet white noise (60dB) was used to drown out background noise and floor lamps were used for low-level ambient lighting.

On the first day, each animal underwent a habituation session consisting of 1min inside a transport bin under the table, 2min underneath the start box in the center of the table, and 3 min inside the hidden tunnel with five sucrose pellets. During training, each rat was assigned a specific escape hole according to the position of the spatial cues with the location counterbalanced across groups. Before each trial, animals were placed in the start box for 30 seconds. Animals were trained over the course of two 5-min trials per day for four days (five days in contralesional experiments) to learn to use the spatial cues in order to locate the correct hole with the hidden tunnel with sucrose pellets. After finding the correct hole and entering the hidden tunnel during each 5min training session, animals were allowed to remain in the hidden tunnel for 1 minute, and consistently consumed all five sucrose pellets at this time. Learning during training was scored via animal head location tracking by AnyMaze Behavior Tracking Software (Stoelting Co., Wood Dale, IL). The incorrect hole investigations prior to finding the correct hole with sucrose pellets (“errors before correct hole”) as well as time to finding the correct hole (“latency to correct hole”) were calculated as an average of the two trials per day and examined across days of training. After the conclusion of training, rats had a two-day break where no procedures occurred, then were tested in a single 2min memory probe in which the hidden tunnel and sucrose pellets were removed.

In the event that a rat did not find the correct hole during the 3min training session, the experimenter gently guided the rat to the correct hole and were allowed to crawl in and then complete the training in the same fashion as rats that found the hole on their own. During training sucrose pellets were taped underneath all of the holes to preclude olfactory-based search strategies during training. Importantly, the memory probe test does not include any sucrose pellets in the apparatus at all, and therefore there is no possibility of sucrose odor cues to influence memory probe performance.

In the memory probe, the ratio of the correct hole plus adjacent hole investigations over the total number of hole investigations were calculated via animal head location tracking by AnyMaze Behavior Tracking Software. This dependent variable was selected a priori instead of correct hole only investigations based on the spatial resolution of rodent hippocampal place cells which ranges from inches to meters depending on the subregion targeted (Kjelstrup et al., 2008) and recent findings demonstrating that taste-responsive hippocampal neurons exhibit weaker spatial selectivity in comparison to non-taste-responsive hippocampal neurons (Herzog et al., 2019). This biological range is better represented by a geometric plane that includes 3/18 circumference space versus 1/18 as we have previously reported (Suarez et al., 2018).

When establishing and refining the food-reinforced spatial memory procedure in multiple cohorts of rats, our preliminary data revealed that memory probe effects in normal/control animals are either stronger in the 1<sup>st</sup> minute, or in the 1<sup>st</sup> two minutes combined (but not the 2<sup>nd</sup> minute alone), with some cohorts showing larger paradigm effects in minute 1, and others in minutes 1+2. Thus, for all experiments presented we analyzed both the 1<sup>st</sup> minute and the 1<sup>st</sup> two minutes combined based on time at which paradigm effect is the strongest.

**Intracranial injections**—Rats were anesthetized via an intramuscular injection of an anesthesia cocktail (ketamine 90mg/kg body weight [BW], xylazine, 2.8mg/kg BW and acepromazine and 0.72mg/kg BW) followed by a pre-operative, subcutaneous injection of analgesic (ketoprofen, 5mg/kg BW). Post-operative analgesic (subcutaneous injection of ketoprofen, 5mg/kg BW) was administered once per day for 3 days following surgery. The surgical site was shaved and prepped with iodine and ethanol swabs, and animals were placed in a stereotaxic apparatus for stereotaxic injections. NMDA or viruses were delivered using a microinfusion pump (Harvard Apparatus, Cambridge, MA) connected to a 33-gauge microsyringe injector attached to a PE20 catheter and Hamilton syringe. Flow rate was calibrated and set to 83.3nL/sec. Injectors were left in place for 2min post-injection to allow for complete delivery of the infusate. Specific viruses/drugs, coordinates, and injection volumes for procedures are detailed below. Following the completion of all injections, incision sites were closed using either surgical staples, or in the case of subsequent placement of an indwelling cannula, simple interrupted sutures. Upon recovery from anesthesia and return to dorsal recumbency, animals were returned to the home cage. All behavioral procedures occurred 21 days after injections to allow for complete transduction and expression of the viruses, or complete lesioning drugs. General intracranial injection procedures were followed for all injection procedures below.

**Fiber photometry**—To record bulk calcium-dependent activity in the HPCv, one group of animals (n = 6) received a bilateral injection of a virus driving expression of the calcium indicator GCaMP7s (AAV9-hSyn-GCaMP7s-WPRE; Addgene; 300nL per side) targeting the CA1v at the following stereotaxic coordinates: -4.9mm AP, +/-4.8mm ML, defined at bregma and -7.8mm DV, defined at skull site. A fiber-optic cannula (Doric Lenses Inc, Quebec, Canada) was implanted at the injection site and affixed to the skull with jeweler's screws, instant adhesive glue, and dental cement.

Photometry recording sessions occurred during the probe trial of the appetitive spatial food seeking memory task (when no food is present) and lasted 3 minutes (1 min acclimation and 2 min probe trial). Photometry signal was acquired using the Neurophotometrics fiber photometry system (Neurophotometrics, San Diego, CA) at a sampling frequency of 40Hz and calcium-dependent signal (470nm) was corrected in MatLab by subtracting the isosbestic (415nm) value and fitting the result to a biexponential curve. Corrected fluorescence signal was then normalized within each rat by calculating the  $F/F$  using the average fluorescence signal for the entire recording. The data was paired with real-time localization of the animal obtained from the AnyMaze Behavior Tracking Software (Stoelting, Wood Dale, IL) using an original MatLab code and each investigation at least 5 seconds apart were isolated for analysis. Z-scores were obtained by normalizing  $F/F$  up to 5 seconds following an investigation to the  $F/F$  at the onset of the investigation (time 0s).

**Chronic lesions of the HPCv**—Lesion animals ( $n = 18$ ) received bilateral excitotoxic HPCv lesions via intracranial injections of N-methyl-d-aspartate (NMDA, Sigma, St-Louis, MO; 4 $\mu$ g in 200nL; 100uL per hemisphere) at the following coordinates at three different sites along the rostro-caudal extent of the HPCv: [1]  $-4.8\text{mm AP}$ ,  $+/-5.0\text{mm ML}$ ,  $-7.5\text{mm DV}$ , [2]  $-5.5\text{mm AP}$ ,  $+/-4.5\text{mm ML}$ ,  $-7.0\text{mm DV}$ , and [3]  $-6.1\text{mm AP}$ ,  $+/-4.8\text{mm ML}$ ,  $-7.0\text{mm DV}$  with control animals ( $n = 11$ ) receiving vehicle saline in the same location. The reference points for AP and ML coordinates were defined at bregma, and the reference point for the DV coordinate was defined at the skull surface at the target site.

Bilateral HPCv lesion brains were histologically evaluated for the correct placement of lesions in 1 out of 5 series of brain tissue sections. Neurons were visualized using immunohistochemistry for the neuron specific antigen NeuN (see Immunohistochemistry). The extent of NMDA lesions was determined postmortem by immunohistochemical detection of the neuronal marker NeuN. Rats showing pronounced ( $\sim 65\%$ ) loss of NeuN labeling within the target region compared with the representative NeuN expression following sham injections in the control group (average HPCv count of NeuN+ cells in control group) were included in data analysis.

**Acute and chronic disconnection models**—Cre-dependent dual viral strategies were used to generate the following groups: [1] acute chemogenetic disconnection of the CA1v to LS neural pathway (DREADDs), [2] chronic disconnection of the CA1v to LS neural pathway (caspase lesion-induced), and [3] a common/shared control group for these two disconnection strategies. Regardless of group, all animals received a bilateral AAV retro-cre injection in the LS (AAV2[retro]-hSYN1-EGFP-2A-iCre-WPRE; Vector BioLabs; 200nL per side) at the following stereotaxic coordinates:  $+0.84\text{mm AP}$ ,  $+/-0.5\text{mm ML}$ ,  $-4.8\text{mm DV}$ , all defined at bregma. According to experimental group, animals received a different virus delivered to the CA1v subregion of the HPCv at the following coordinates:  $-4.9\text{mm AP}$ ,  $+/-4.8\text{mm ML}$ , defined at bregma and  $-7.8\text{mm DV}$ , defined at skull site.

**[1] DREADDs group for reversible inactivation of CA1v to LS:** To allow reversible chemogenetic inactivation of the CA1v to LS neural pathway, one group of animals received a bilateral CA1v injection of a Cre-dependent virus to drive expression of inhibitory designer receptors activated by designer drugs (DREADDs), (AAV-Flex-hM4Di-

mCherry; Addgene; 200nL per side). This dual viral strategy drives expression of inhibitory DREADDs exclusively in LS-projecting CA1v neurons, which enables acute inactivation of these neurons by injection of the DREADDs ligand, clozapine-N-oxide (CNO), at the time of behavioral testing.

**[2] Caspase group for chronic inactivation of CA1v to LS:** To allow chronic disconnection of the CA1v to LS neural pathway, a second group of animals received a bilateral CA1v Cre-dependent caspase virus (AAV1-Flex-taCasp3-TEVp; UNC Vector Core; 200nL per side) mixed with a Cre-dependent reporter virus (AAV-CAG-Flex-tdTomato-WPRE-bGH, UPenn Vector Core; 200nL per side) for histological verification. This dual viral strategy drives expression of the apoptosis-mediator molecule caspase exclusively in LS-projecting CA1v neurons, which induces apoptotic cell death in these neurons while leaving other CA1v neurons intact.

**[3] Common control:** A common control group was used for the DREADDs and caspase groups. This allowed us to reduce the number of animals needed for the same experimental objective. Thus, all animals received an indwelling cannula and ICV injections of CNO as described below.

Immediately following viral injections, all animals were surgically implanted with a unilateral indwelling intracerebroventricular (ICV) cannula (26-gauge, Plastics One, Roanoke, VA) targeting the lateral ventricle (VL). Cannulae were implanted and affixed to the skull with jeweler's screws and dental cement at the following stereotaxic coordinates: -0.9mm AP defined at bregma, +1.8mm ML defined at bregma, -2.6mm DV defined at skull surface at site.

**Validation of inhibitory DREADDs expression—**Cre-dependent DREADD expression targeting LS-projecting neurons in CA1v was evaluated based on localization of the fluorescent reporter mCherry. Immunohistochemistry for red fluorescent protein (RFP) was conducted to amplify the mCherry signal (see Immunohistochemistry). Only animals with mCherry expression restricted within CA1v neurons were included in subsequent behavioral analyses. The same approach was used to validation of inhibitory DREADDs expression for the CA1v-mPFC experiment.

**Validation of caspase-mediated disconnection—**The general approach for neuronal apoptosis due to activation of Cre-dependent caspase targeting LS-projecting neurons in CA1v was validated in a separate cohort (n = 8) based on reduction of a Cre-dependent fluorescent reporter tdTomato due to neuron cell death compared with controls. The caspase group brains (which received a retro-cre virus in the LS in conjunction with an injection of Cre-dependent caspase virus mixed with a Cre-dependent virus that drives a tdTomato fluorescent reporter in the CA1v) were compared to control brains (that received a retro-cre virus in the LS in conjunction with only a Cre-dependent that drives a tdTomato fluorescent reporter in the CA1v, which was equivalently diluted to match the caspase injections). In both groups, immunohistochemistry for red fluorescent protein (RFP) was conducted to amplify the tdTomato signal (see Immunohistochemistry). Confirmation of successful caspase-driven lesions in the CA1v using this approach was evaluated by reduced tdTomato

fluorescence in comparison to control animals, with the expression of CA1v tdTomato expression in the caspase group less than 15% of that observed in controls, on average. While this cohort allowed for successful validation of the pathway-specific disconnection caspase approach, to improve the viability of the animals for long-term behavioral analyses, the 3<sup>rd</sup> AAV with the fluorescent reporter (Cre-dependent tdTomato AAV) was omitted for cohorts undergoing behavioral analyses. For these groups, histological confirmation for inclusion in subsequent statistical analyses was based on identification of injections sites confined with the LS and CA1v, as observed using darkfield microscopy.

**Validation of ICV cannula placement**—Placement for the VL cannula was verified by elevation of blood glucose resulting from an injection of 210 $\mu$ g (2 $\mu$ L) of 5-thio-D-glucose (5TG) using an injector that extended 2mm beyond the end of the guide cannula (Ritter et al., 1981). A post-injection elevation of at least 100% of baseline glycemia was required for subject inclusion. Animals that did not pass the 5TG test were retested with an injector that extended 2.5mm beyond the end of the guide cannula and, upon passing the 5TG test, were subsequently injected using a 2.5mm injector instead of a 2mm injector for the remainder of the study.

**ICV CNO infusion**—Administration route for CNO (RTI International) and dosage were determined based on previous publications demonstrating reliable DREADDs activation (Hsu et al., 2018b; Noble et al., 2018; Terrill et al., 2020). Prior to behavioral testing where noted, all animals received an ICV 18mmol infusion (2 $\mu$ L total volume) of the DREADDs ligand clozapine N-oxide (CNO), rendering only DREADDs animals chemogenetically inactivated. CNO injections were hand delivered using a 33-gauge microsyringe injector attached to a PE20 catheter and Hamilton syringe through the indwelling guide cannula. Injectors were left in place for 30sec to allow for complete delivery of the CNO.

**Appetitive water seeking spatial memory task**—We modified our spatial food seeking task to utilize water reward instead of food reward. Throughout this paradigm, animals were water restricted and received 90-min access to water daily (given at least 1hr after the termination of behavioral procedures each day). In addition to the habituation parameters described above, animals in this task were subjected to two 10-min habituation sessions in the hidden tunnel with a full water dish prior to training, which allowed them to become accustomed to reliably drinking from the water dish in the hidden tunnel. Training procedures were the same as for the food-based task above, except instead of sucrose pellets in the hidden tunnel, a water dish containing ~100 mL of water was placed in the back of the hidden tunnel during training, and animals were allowed to remain in the hidden tunnel for 2min (instead of 1min, as above). Each animal consumed a minimum of 2mL of water during this time for the training sessions. This adapted procedure allowed us to test spatial learning and memory motivated by water reward using similar apparatus and stimulus conditions to the food-reinforced task.

**Aversive spatial memory escape task (Barnes maze)**—To test visuospatial learning and memory for escape-based reinforcement, we used a modified traditional Barnes maze procedure, which is a visuospatial escape task (Barnes, 1979). Procedures were the same

as above (appetitive spatial memory food seeking and water seeking tasks, using the same apparatus, in the same room, and with the same visuospatial cues) aside from the omission of the sucrose pellets or water dish in the hidden tunnel, the presence of mildly aversive bright (120W) overhead lighting instead of dim ambient lighting, and a mildly aversive loud white noise (75dB) instead of a quiet white noise (60dB). This allowed us to test spatial learning and memory motivated by escape from aversive stimuli in a nearly identical procedure to our spatial foraging test for learning and memory motivated by palatable food or water consumption.

**Identification of CA1v to LS collateral targets**—Collateral targets of the CA1v to LS neural pathway were identified using a dual viral approach where a retrograde vector was injected into the LS (AAV2retro-hSyn1-eGFP-2A-iCre-WPRE; Vector BioLabs; 200nL per side), and a Cre-dependent anterograde vector (AAV1-CAG-Flex-tdTomato-WPRE-bGH, UPenn Vector Core; 200nL per side) was injected in the CA1v. This latter injection drives tdTomato transgene expression in CA1v neurons that project to the LS, which allows for brain-wide analyses of collateral targets. After 3 weeks of incubation time to allow for complete transduction and expression of the viruses, brains were collected, immunohistochemically processed, and imaged as described below.

**Acute CA1v to mPFC disconnection**—To functionally disconnect the CA1v to mPFC pathway (diagram of approach in Figure 3C) a group of animals all received bilateral AAV retro-cre injection in the mPFC (AAV2[retro]-hSYN1-EGFP-2A-iCre-WPRE; Vector BioLabs; 200nL per side) at the following stereotaxic coordinates: +2.7mm AP, +/- 0.5mm ML and -4.3mm DV, all defined at bregma. The same animals also received bilateral infusion of a Cre-dependent inhibitory DREADDs (AAV-Flex-hM4Di-mCherry; Addgene; 200nL per side) in the CA1v at the following stereotaxic coordinates: -4.9mm AP, +/- -4.8mm ML, defined at bregma and -7.8mm DV, defined at skull site. Finally, all these animals were additionally implanted with a unilateral indwelling ICV cannula as described for the previous cohorts at the following stereotaxic coordinates: -0.9mm AP defined at bregma, +1.8mm ML defined at bregma, -2.6mm DV defined at skull surface at site. Prior to the memory probe (1h), animals received an ICV 18mmol infusion of CNO (n = 8) or its vehicle (aCSF; n = 6).

**Food intake and body weight**—For the day prior to surgery (day 0) and for two weeks thereafter, 24h chow intake was measured daily just prior to dark cycle onset to determine effects of experimental procedures on food intake. Spillage was accounted for daily by collecting crumbs onto Techboard paper placed under the cages of each animal. Additionally, animals were weighed daily just prior to dark cycle onset to determine effects of experimental procedures on body weight.

**Meal pattern analysis**—Meal size, meal frequency, meal duration, and cumulative 24h food intake were measured using Biodaq automated food intake monitors (Research Diets, New Brunswick, NJ). Rats were acclimated to the Biodaq on ad libitum chow for 3 days. Caspase group (n = 7) vs. control group (n = 7) feeding behavior data were collected over a 5-day period (untreated, between-subjects design). The DREADDs group was tested using

a 2-treatment within-subjects design. Rats (n = 8) received 18mmol infusion of ICV CNO (2uL total volume) or vehicle (aCSF, 33% dimethyl sulfoxide in artificial cerebrospinal fluid) 1h prior to lights off and 24h feeding behavior was measured. Meal parameters were set at minimum meal size = 0.2g and maximum intermeal interval = 600s.

**Operant responding for sucrose rewards**—Rats expressing inhibitory DREADDs in CA1v-to-LS projections and implanted with an ICV cannula (n = 6) were trained to lever press for 45mg sucrose pellets (cat. no. F0023, Bio-Serv) over the course of 6 days with a 1h session each day (2 days of fixed ratio 1 with autoshaping procedure, 2 days of fixed ratio 1 and 2 days of fixed ratio 3 reinforcement schedule) in operant conditioning boxes (Med Associates Inc, St. Albans, VT). Over two treatment days separated by 48h, rats were placed back in the operant chambers to lever press for sucrose under a progressive ratio reinforcement schedule, 1h following ICV infusion (2uL) of 18mmol CNO or aCSF, with both treatments administered to each rat in a counter-balanced manner (within-subject). The response requirement increased progressively using the following formula:  $F(i) = 5e^{0.2i-5}$ , where  $F(i)$  is the number of lever presses required for the next pellet at  $i$  = pellet number and the breakpoint was defined as the final completed lever press requirement that preceded a 20-min period without earning a reinforcer, as described previously (Hsu et al., 2015a).

**Social transmission of food preference (STFP)**—To examine food-related memory based on social- and olfactory-based cues, we utilized the social transmission of food preference (STFP) task and adapted protocols from (Countryman and Gold, 2007; Countryman et al., 2005; Hsu et al., 2018a). Briefly, untreated normal adult rats were designated as ‘Demonstrators’, while experimental groups were designated as ‘Observers’. Demonstrators and Observers were habituated to a powdered rodent chow [LabDiet 5001 (ground pellets), LabDiet, St. Louis, MO] overnight. 24h later, Observers were individually paired with demonstrators and habituated to social interaction, where rat pairs were placed in a social interaction arena (23.5cm W × 44.45cm L × 27cm H clear plastic bin with Sani-chip bedding) and allowed to interact for 30min. Both Observers and Demonstrators were returned to their home cages and food was withheld for 23hr prior to the social interaction. For the social interaction, Demonstrators were given the opportunity to consume one of two flavors of powdered chow (flavored with 2% marjoram or 0.5% thyme; counterbalanced according to group assignments) for 30min in a room separate from Observers. Our pilot studies and previous published work (Galef and Whiskin, 2003; Galef et al., 2005) showed that rats equally prefer these flavors of chow. The Demonstrator rat was then placed in the social interaction arena with the Observer rat, and the pairs were allowed to socially interact for 30min. Observers were then returned to their home cage and allowed to eat *ad libitum* for 1h and then food was removed. The following day, the 23h food-deprived Observer animals were given a home cage food preference test for either the flavor of chow paired with the Demonstrator animal, or a novel, unpaired flavor of chow that is a flavor that was not given to the Demonstrator animal (2% marjoram vs. 0.5% thyme; counterbalanced according to group assignments). All animals received an ICV 18mmol infusion of CNO (2uL total volume) 1h prior to the social interaction session, rendering only DREADDs animals chemogenetically inactivated by CNO. Food intake (1h) was recorded with spillage accounted for by collecting crumbs onto Techboard paper that was placed

under the cages of each animal. The % preference for the paired flavor was calculated as:  $100 \times \text{Demonstrator-paired flavored chow intake} / (\text{Demonstrator} + \text{Novel flavored chow intake})$ . In this procedure, normal untreated animals learn to prefer the Demonstrator paired flavor based on social interaction and smelling the breath of the Demonstrator rat (Countryman and Gold, 2007; Countryman et al., 2005; Galef and Whiskin, 2003; Galef et al., 2005; Hsu et al., 2018a).

**Zero maze**—The zero maze behavioral paradigm was used to evaluate anxiety-like behavior. The zero maze apparatus used was an elevated circular track, divided into four equal length sections. Two zones were open with 3 cm high curbs ('open zones'), whereas the two other zones were closed with 17.5 cm high walls ('closed zones'). All animals received an ICV 18mmol infusion of CNO (2uL total volume) 1h prior to testing, rendering only DREADDs animals chemogenetically inactivated by CNO. Behavioral testing was performed during the light cycle. Animals were placed in the maze for a single, 5min trial in which the location of the center of the animal's body was measured by AnyMaze Behavior Tracking Software (Stoelting). The apparatus was cleaned with 10% ethanol in between animals. During the trial, the number of open zone entries and total time spent in open sections (defined as body center in open sections) were measured, which are each indicators of anxiety-like behavior in this procedure.

**Open field**—An open field test was used to evaluate general levels of locomotor activity. The apparatus used for the open field test was an opaque gray plastic bin (60 cm × 56 cm), which was positioned on a flat table in an isolated room with a camera directly above the center of the apparatus. Desk lamps were positioned to provide indirect lighting to all corners of the maze such that the lighting in the box uniformly measured 30 lux throughout. All animals received an ICV 18mmol infusion of CNO (2uL total volume) 1h prior to testing rendering only DREADDs animals chemogenetically inactivated by CNO. Behavioral testing began at dark onset. At the start of the 10min test, each animal was placed in the open field apparatus in the same corner facing the center of the maze. The location of the center of the animal's body was measured with the AnyMaze Behavior Tracking Software (Stoelting). Total distance traveled was measured by tracking movement from the center of the animal's body throughout the test.

**c-Fos+ FISH neurotransmitter phenotyping**—Activation of LS neurons from the spatial memory probe test was confirmed with c-Fos immunoreactivity analyses. Animals receiving the DREADDs-mediated treatment for reversible inactivation of CA1v to LS signaling underwent training in the appetitive food seeking memory task (conducted as described above). One hour before the memory probe, animals received ICV injection of CNO (n = 4) or vehicle (aCSF; n = 4). Animals were tested in the memory probe and perfused with tissue harvest 90 min later. Fluorescent *in situ* hybridization analyses for c-Fos (cat. no. 403591, ACD, Newark, CA), ChAT (cat. no. 430111, ACD), GAD1 (cat. no. 316401, ACD), and vGLUT2 (cat. no. 317011, ACD) were performed, and co-localization of c-Fos positive cells and individual neurotransmitter markers was quantitatively analyzed for a subset of rats (n = 3) in the vehicle treated group.

**Identification of second-order targets**—To identify second order targets of CA1v to LS-projecting neurons, animals received a bilateral injection of a transsynaptic Cre-inducing anterograde vector into CA1v (AAV1-hSyn-Cre-WPRE-hGH, UPenn Vector Core; 200nL per side; coordinates as above) that drives expression of Cre in both first-order (CA1v injection site) and 2<sup>nd</sup>-order (but not 3<sup>rd</sup>-order) neurons via transsynaptic virion release (Suarez et al., 2018; Zingg et al., 2017). This was combined with a bilateral injection of a Cre-dependent anterograde vector in the LS (AAV1-CAG-Flex-tdTomato-WPRE-bGH, UPenn Vector Core; 200nL per side, coordinates as above). This latter injection allows for anterograde tracing from 1<sup>st</sup>-order LS targets receiving synaptic input from CA1v. After 3 weeks of incubation time to allow for complete transduction and expression of the viruses, brains were collected, immunohistochemically processed, and imaged as described below.

Data were entered using a custom built data-entry platform (Axiome C, created by JDH) built around Microsoft Excel software and designed to facilitate entry of data points for all gray matter regions across their atlas levels as described in a rat brain reference atlas: Brain Maps 4.0 (Swanson, 2018). The Axiome C approach was used previously to facilitate the analysis of brain gene-expression data (Hahn et al., 2019). An ordinal scale, ranging from 0 (absent) to 7 (very strong), was used to record the qualitative weight of anterograde labeling. An average value was then obtained for each region across its atlas levels for which data were available. These data are summarized graphically for a representative animal on a brain flatmap summary diagram (adapted from (Hahn et al., 2021)).

The LHA was identified as a primary downstream target of the CA1v to LS pathway from the analyses described above. In order to further confirm this conclusion, an additional co-injection monosynaptic neural tracing strategy (COIN; (Suarez et al., 2018; Thompson and Swanson, 2010)) was conducted. Animals (n = 6) received unilateral pressure injections of AAV1-GFP (AAV1-hSyn-eGFP-WPRE-bGH; Vector BioLabs; anterograde tracer) targeting the CA1v and, in the same animal, fluorogold (Fluorochrome; retrograde tracer) targeting the LHA (injection coordinates described above). Following a 10-day incubation period, animals were fixation-perfused and tissue was collected and processed as described below. Injection sites were confined to the CA1v (AAV1) and LHA (FG) in the same animal (“double hits”, n = 4). Appositions between FG and GFP were examined in the LS in these animals by visualizing native GFP and FG fluorescence and the percentage of FG cells in direct contact with GFP CA1v-originating axons was quantified (n = 4).

To verify if acute silencing of the CA1v to LS neuronal pathway reduces neuronal activity in the LHA, staining against c-Fos was performed on coronal LHA slices from animals with expression of inhibitory DREADDs in CA1v to LS neurons and infused with CNO (n = 4) or vehicle (aCSF; n = 4) 1h prior to the memory probe. Counts of c-Fos+ cells were done in the 2 subregions of the LHA found to receive the highest density of projections from CA1v neurons (LHAjd and LHAjv). In another series of LHA coronal sections from the same animals, counts of c-Fos+ cells were done in orexin+ or MCH+ neurons (see Immunohistochemistry).

Counts of c-Fos+ cells were also done in LHA coronal sections from rats treated with CNO (n = 6) and aCSF (n = 4) lacking expression of inhibitory DREADDs as a control experiment.

**Immunohistochemistry**—Rats were anesthetized via an intramuscular injection of an anesthesia cocktail (ketamine 90mg/kg BW xylazine, 2.8mg/kg BW and acepromazine and 0.72mg/kg BW) then transcardially perfused with 0.9% sterile saline (pH 7.4) followed by 4% paraformaldehyde (PFA) in 0.1M borate buffer (pH 9.5; PFA). Brains were dissected from the skull and post-fixed in PFA with 15% sucrose for 24h, then flash frozen in isopentane cooled in dry ice. Brains were sectioned to 30µm thickness on a freezing microtome. Sections were collected in 5-series and stored in antifreeze solution at -20°C until further processing. General fluorescence IHC labeling procedures were performed as follows. The antibodies and dilutions that were used are as follows: [1] For lesion histology using the neuron-specific protein NeuN, the rabbit anti-NeuN primary antibody (1:1000, Abcam, Boston, MA) was used followed by a donkey anti-rabbit conjugated to AF488 (1:500, Jackson ImmunoResearch, West Grove, PA). [2] To amplify the native tdTomato signal for neuroanatomical tracing or DREADDs histology, the rabbit anti-RFP primary antibody (1:2000, RRID: AB\_2209751, Rockland, Limerick, PA) was used followed by a donkey anti-rabbit conjugated to Cy3 (1:500, Jackson ImmunoResearch). [3] To amplify the native GFP signal for LS injection site histology, the chicken anti-GFP primary antibody (1:500, Abcam) was used followed by a donkey anti-chicken secondary antibody conjugated to AF488 (1:500, Jackson ImmunoResearch). [4] To validate that the acute disconnection approach reduced neuronal activity in the LS and LHA, the mouse anti-c-Fos primary antibody (1:1000, Ab208942, Abcam) was used followed by a donkey anti-mouse secondary antibody conjugated to AF647 (1:500, Jackson ImmunoResearch). To identify the neuropeptide population in which LHA c-Fos is expressed following the foraging spatial memory probe, the rabbit anti-orexin (1:5000, AB3704, EMD Millipore, Burlington, MA) or anti-MCH (1:10000, H\_070\_47, Phoenix Pharmaceuticals, Burlingame, CA) primary antibody was also used followed by a donkey anti-rabbit secondary antibody conjugated to AF488 (1:500, Jackson ImmunoResearch).

Antibodies were prepared in 0.02M potassium phosphate buffered saline (KPBS) solution containing 0.2% bovine serum albumin and 0.3% Triton X-100 at 4°C overnight. After thorough washing with 0.02M KPBS, sections were incubated at 4°C overnight in secondary antibody solution. Sections were mounted and coverslipped using 50% glycerol in 0.02 M KPBS and the edges were sealed with clear nail polish. Photomicrographs were acquired using a Nikon 80i (Nikon DSQI1, 1280X1024 resolution, 1.45 megapixel) under epifluorescence or darkfield illumination.

Lesions and virus expression were quantified in one out of five series of brain tissue sections and analyses were performed in sections from Swanson Brain Atlas level 34–36 (Swanson, 2018). The inclusion/exclusion criteria are described above in the methods of each of these experiments.

## QUANTIFICATION AND STATISTICAL ANALYSIS

Data are expressed as mean  $\pm$  SEM, statistical details can be found in the figure legends and n's refer to the number of animals for each condition. Differences were considered statistically significant at  $p < 0.05$ . All variables were analyzed using the advanced analytics software package Statistica (StatSoft, Tulsa, OK, USA).

A simple linear regression analysis was performed to illustrate the relationship between variation in z-score to distance from escape hole. A two-tailed paired two-sample Student's t-test was used to compare delta z-score 5 seconds following a correct versus incorrect investigation and meal pattern analysis and operant responding for sucrose rewards in response to treatment in the model of acute disconnection of the CA1v to LS pathway. For measures during memory probes in the HPCv lesion and CA1v-mPFC experiments, 5-day averages for meal pattern analysis in the model of chronic disconnection and c-Fos counts following administration of CNO or aCSF, differences between groups were evaluated using two-tailed independent two-sample Student's t-tests. For CA1v to LS acute and chronic disconnection experiments, measures during spatial foraging and spatial escape task probes, the STFP paradigm, the zero maze paradigm, and the open field test, differences between groups were evaluated using one-way ANOVAs. For the variation in photometry signal across time, meal pattern analysis for the chronic disconnection model and all measures of food intake, body weight, and errors/latency during spatial foraging and spatial escape task training, differences between groups were evaluated using two-way repeated measures ANOVAs (treatment  $\times$  time). Significant ANOVAs were analyzed with a Fisher's LSD posthoc test where appropriate. For all memory probes, as well as the STFP, one-sample t-tests were conducted to determine whether performance was significantly different from chance set at 0.1667 and 0.5, respectively. Outliers were identified as being more extreme than the median  $\pm 1.5$  \* interquartile range. For all experiments, assumptions of normality, homogeneity of variance (HOV), and independence were met where required.

## Supplementary Material

Refer to Web version on PubMed Central for supplementary material.

## ACKNOWLEDGMENTS

This work was supported by a Fonds de Recherche du Québec Postdoctoral Fellowship to L.D.-S. (315201), a National Science Foundation Graduate Research Fellowship to K.S., and by National Institute of Diabetes and Digestive and Kidney Diseases grants DK104897 and DK118402 to S.E.K., DK118944 to C.M.L., DK116558 to A.N.S., and DK118000 to E.E.N. CNO was kindly provided by the National Institute of Mental Health. The authors are grateful to the Kanoski lab undergraduate research assistants for their assistance in behavioral experiments and histology, and to Jini Park for the creation of the graphical abstract.

## REFERENCES

- Aqrabawi AJ, and Kim JC (2018). Topographic organization of hippocampal inputs to the anterior olfactory nucleus. *Front. Neuroanat* 12, 12. [PubMed: 29520221]
- Aqrabawi AJ, Browne CJ, Dargaei Z, Garand D, Khademullah CS, Woodin MA, and Kim JC (2016). Top-down modulation of olfactory-guided behaviours by the anterior olfactory nucleus pars medialis and ventral hippocampus. *Nat. Commun* 7, 13721. [PubMed: 28004701]

- Arszovszki A, Borhegyi Z, and Klausberger T (2014). Three axonal projection routes of individual pyramidal cells in the ventral CA1 hippocampus. *Front. Neuroanat* 8, 53. [PubMed: 25009471]
- Barnes CA (1979). Memory deficits associated with senescence: a neurophysiological and behavioral study in the rat. *J. Comp. Physiol. Psychol* 93, 74–104. [PubMed: 221551]
- Barson JR, Morganstern I, and Leibowitz SF (2013). Complementary roles of orexin and melanin-concentrating hormone in feeding behavior. *Int. J. Endocrinol*, 983964. [PubMed: 23935621]
- Bienkowski MS, Bowman I, Song MY, Gou L, Ard T, Cotter K, Zhu M, Benavidez NL, Yamashita S, Abu-Jaber J, et al. (2018). Integration of gene expression and brain-wide connectivity reveals the multiscale organization of mouse hippocampal networks. *Nat. Neurosci* 21, 1628–1643. [PubMed: 30297807]
- Carballo-Márquez A, Vale-Martínez A, Guillazo-Blanch G, and Martí-Nicolovius M (2009). Muscarinic receptor blockade in ventral hippocampus and prelimbic cortex impairs memory for socially transmitted food preference. *Hippocampus* 19, 446–455. [PubMed: 19004013]
- Carus-Cadavieco M, Gorbati M, Ye L, Bender F, Van Der Veldt S, Kosse C, Börgers C, Lee SY, Ramakrishnan C, Hu Y, et al. (2017). Gamma oscillations organize top-down signalling to hypothalamus and enable food seeking. *Nature* 542, 232–236. [PubMed: 28146472]
- Contreras M, Pelc T, Llofriu M, Weitzenfeld A, and Fellous JM (2018). The ventral hippocampus is involved in multi-goal obstacle-rich spatial navigation. *Hippocampus* 28, 853–866. [PubMed: 30067283]
- Countryman RA, and Gold PE (2007). Rapid forgetting of social transmission of food preferences in aged rats: relationship to hippocampal CREB activation. *Learn. Mem* 14, 350–358. [PubMed: 17522026]
- Countryman RA, Kaban NL, and Colombo PJ (2005). Hippocampal c-fos is necessary for long-term memory of a socially transmitted food preference. *Neurobiol. Learn. Mem* 84, 175–183. [PubMed: 16122949]
- Fanselow MS, and Dong HW (2010). Are the dorsal and ventral hippocampus functionally distinct structures? *Neuron* 65, 7–19. [PubMed: 20152109]
- Ferbinteanu J, Ray C, and McDonald RJ (2003). Both dorsal and ventral hippocampus contribute to spatial learning in Long-Evans rats. *Neurosci. Lett* 345, 131–135. [PubMed: 12821188]
- Galef BG, and Whiskin EE (2003). Socially transmitted food preferences can be used to study long-term memory in rats. *Learn. Behav* 31, 160–164. [PubMed: 12882374]
- Galef BG, Lee WY, and Whiskin EE (2005). Lack of interference in long-term memory for socially learned food preferences in rats (*Rattus norvegicus*). *J. Comp. Psychol* 119, 131–135. [PubMed: 15982156]
- Garcia R, Vouimba RM, and Jaffard R (1993). Spatial discrimination learning induces LTP-like changes in the lateral septum of mice. *Neuroreport* 5, 329–332. [PubMed: 8298099]
- Gaskin S, Gamliel A, Tardif M, Cole E, and Mumby DG (2009). Incidental (unreinforced) and reinforced spatial learning in rats with ventral and dorsal lesions of the hippocampus. *Behav. Brain Res* 202, 64–70. [PubMed: 19447282]
- Gergues MM, Han KJ, Choi HS, Brown B, Clausing KJ, Turner VS, Vainchtein ID, Molofsky AV, and Kheirbek MA (2020). Circuit and molecular architecture of a ventral hippocampal network. *Nat. Neurosci* 23, 1444–1452. [PubMed: 32929245]
- Hafting T, Fyhn M, Molden S, Moser MB, and Moser EI (2005). Microstructure of a spatial map in the entorhinal cortex. *Nature* 436, 801–806. [PubMed: 15965463]
- Hahn JD, Sporns O, Watts AG, and Swanson LW (2019). Macroscale intrinsic network architecture of the hypothalamus. *Proc. Natl. Acad. Sci. USA* 116, 8018–8027. [PubMed: 30923123]
- Hahn JD, Swanson LW, Bowman I, Foster NN, Zingg B, Bienkowski MS, Hintiryan H, and Dong HW (2021). An open access mouse brain flatmap and upgraded rat and human brain flatmaps based on current reference atlases. *J. Comp. Neurol* 529, 576–594. [PubMed: 32511750]
- Hannapel R, Ramesh J, Ross A, Lalumiere RT, Roseberry AG, and Parent MB (2019). Postmeal optogenetic inhibition of dorsal or ventral hippocampal pyramidal neurons increases future intake. *ENeuro* 6. ENEURO.0457-18.2018.

- Hannapel RC, Henderson YH, Nalloor R, Vazdarjanova A, and Parent MB (2017). Ventral hippocampal neurons inhibit postprandial energy intake. *Hippocampus* 27, 274–284. [PubMed: 28121049]
- Hauser J, Llano López LH, Feldon J, Gargiulo PA, and Yee BK (2020). Small lesions of the dorsal or ventral hippocampus subregions are associated with distinct impairments in working memory and reference memory retrieval, and combining them attenuates the acquisition rate of spatial reference memory. *Hippocampus* 30, 938–957. [PubMed: 32285544]
- Henke PG (1990). Hippocampal pathway to the amygdala and stress ulcer development. *Brain Res. Bull* 25, 691–695. [PubMed: 2289157]
- Herzog LE, Pascual LM, Scott SJ, Mathieson ER, Katz DB, and Jadhav SP (2019). Interaction of taste and place coding in the Hippocampus. *J. Neurosci* 39, 3057–3069. [PubMed: 30777885]
- Herzog LE, Katz DB, and Jadhav SP (2020). Refinement and reactivation of a taste-responsive hippocampal network. *Curr. Biol* 30, 1306–1311.e4. [PubMed: 32197078]
- Ho AS, Hori E, Nguyen PHT, Urakawa S, Kondoh T, Torii K, Ono T, and Nishijo H (2011). Hippocampal neuronal responses during signaled licking of gustatory stimuli in different contexts. *Hippocampus* 21, 502–519. [PubMed: 20087892]
- de Hoz L, Knox J, and Morris RGM (2003). Longitudinal axis of the hippocampus: both septal and temporal poles of the hippocampus support water maze spatial learning depending on the training protocol. *Hippocampus* 13, 587–603. [PubMed: 12921349]
- Hsu TM, Hahn JD, Konanur VR, Lam A, and Kanoski SE (2015a). Hippocampal GLP-1 receptors influence food intake, meal size, and effort-based responding for food through volume transmission. *Neuropsychopharmacology* 40, 327–337. [PubMed: 25035078]
- Hsu TM, Hahn JD, Konanur VR, Noble EE, Suarez AN, Thai J, Nakamoto EM, and Kanoski SE (2015b). Hippocampus ghrelin signaling mediates appetite through lateral hypothalamic orexin pathways. *Elife* 4, e11190. [PubMed: 26745307]
- Hsu TM, Noble EE, Reiner DJ, Liu CM, Suarez AN, Konanur VR, Hayes MR, and Kanoski SE (2018a). Hippocampus ghrelin receptor signaling promotes socially-mediated learned food preference. *Neuropharmacology* 131, 487–496. [PubMed: 29191751]
- Hsu TM, Noble EE, Liu CM, Cortella AM, Konanur VR, Suarez AN, Reiner DJ, Hahn JD, Hayes MR, and Kanoski SE (2018b). A hippocampus to prefrontal cortex neural pathway inhibits food motivation through glucagon-like peptide-1 signaling. *Mol. Psychiatry* 23, 1555–1565. [PubMed: 28461695]
- Jaffard R, Vouimba RM, Marighetto A, and Garcia R (1996). Long-term potentiation and long-term depression in the lateral septum in spatial working and reference memory. *J. Physiol. Paris* 90, 339–341. [PubMed: 9089509]
- Kanoski SE, and Grill HJ (2017). Hippocampus contributions to food intake control: mnemonic, neuroanatomical, and endocrine mechanisms. *Biol. Psychiatry* 81, 748–756. [PubMed: 26555354]
- Kanoski SE, Hayes MR, Greenwald HS, Fortin SM, Gianessi CA, Gilbert JR, and Grill HJ (2011). Hippocampal leptin signaling reduces food intake and modulates food-related memory processing. *Neuropsychopharmacology* 36, 1859–1870. [PubMed: 21544068]
- Kanoski SE, Fortin SM, Ricks KM, and Grill HJ (2013). Ghrelin signaling in the ventral hippocampus stimulates learned and motivational aspects of feeding via PI3K-Akt signaling. *Biol. Psychiatry* 73, 915–923. [PubMed: 22884970]
- Keinath AT, Wang ME, Wann EG, Yuan RK, Dudman JT, and Muzzio IA (2014). Precise spatial coding is preserved along the longitudinal hippocampal axis. *Hippocampus* 24, 1533–1548. [PubMed: 25045084]
- Kjelstrup KB, Solstad T, Brun VH, Hafting T, Leutgeb S, Witter MP, Moser EI, and Moser MB (2008). Finite scale of spatial representation in the hippocampus. *Science* 321, 140–143. [PubMed: 18599792]
- Kjelstrup KG, Tuvnes FA, Steffenach HA, Murison R, Moser EI, and Moser MB (2002). Reduced fear expression after lesions of the ventral hippocampus. *Proc. Natl. Acad. Sci. USA* 99, 10825–10830. [PubMed: 12149439]

- Kosugi K, Yoshida K, Suzuki T, Kobayashi K, Yoshida K, Mimura M, and Tanaka KF (2021). Activation of ventral CA1 hippocampal neurons projecting to the lateral septum during feeding. *Hippocampus* 31, 294–304. [PubMed: 33296119]
- De La Rosa-Prieto C, Ubeda-Banon I, Mohedano-Moriano A, Pro-Sistiaga P, Saiz-Sanchez D, Insausti R, and Martinez-Marcos A (2009). Subicular and CA1 hippocampal projections to the accessory olfactory bulb. *Hippocampus* 19, 124–129. [PubMed: 18777562]
- Lee SLT, Lew D, Wickenheisser V, and Markus EJ (2019). Interdependence between dorsal and ventral hippocampus during spatial navigation. *Brain Behav* 9, e01410. [PubMed: 31571397]
- Liu J-J, Tsien RW, and Pang ZP (2022). Hypothalamic melanin-concentrating hormone regulates hippocampus-dorsolateral septum activity. *Nat. Neurosci* 25, 61–71. [PubMed: 34980924]
- Lord MN, Subramanian K, Kanoski SE, and Noble EE (2021). Melanin-concentrating hormone and food intake control: sites of action, peptide interactions, and appetite. *Peptides* 137, 170476. [PubMed: 33370567]
- Mani BK, Walker AK, Lopez Soto EJ, Raingo J, Lee CE, Perelló M, Andrews ZB, and Zigman JM (2014). Neuroanatomical characterization of a growth hormone secretagogue receptor-green fluorescent protein reporter mouse. *J. Comp. Neurol* 522, 3644–3666. [PubMed: 24825838]
- Maske CB, Loney GC, Lilly N, Terrill SJ, and Williams DL (2018). Intragastric nutrient infusion reduces motivation for food in male and female rats. *Am. J. Physiol. Endocrinol. Metab* 315, E81–E90. [PubMed: 29533738]
- Merchenthaler I, Lane M, and Shughrue P (1999). Distribution of pre-proglucagon and glucagon-like peptide-1 receptor messenger RNAs in the rat central nervous system. *J. Comp. Neurol* 403, 261–280. [PubMed: 9886047]
- Morris R (1984). Developments of a water-maze procedure for studying spatial learning in the rat. *J. Neurosci. Methods* 11, 47–60. [PubMed: 6471907]
- Morris RGM (1997). Hippocampal synaptic plasticity: role in spatial learning or the automatic recording of attended experience? In *Philosophical Transactions of the Royal Society B: Biological Sciences* (The Royal Society), pp. 1489–1503.
- Moser MB, and Moser EI (1998). Functional differentiation in the hippocampus. *Hippocampus* 8, 608–619. [PubMed: 9882018]
- Noble EE, Hahn JD, Konanur VR, Hsu TM, Page SJ, Cortella AM, Liu CM, Song MY, Suarez AN, Szujewski CC, et al. (2018). Control of feeding behavior by cerebral ventricular volume transmission of melanin-concentrating hormone. *Cell Metab* 28, 55–68.e7. [PubMed: 29861386]
- O'Connor EC, Kremer Y, Lefort S, Harada M, Pascoli V, Rohner C, and Lüscher C (2015). Accumbal D1R neurons projecting to lateral hypothalamus authorize feeding. *Neuron* 88, 553–564. [PubMed: 26593092]
- O'Keefe J, and Dostrovsky J (1971). The hippocampus as a spatial map. Preliminary evidence from unit activity in the freely-moving rat. *Brain Res* 34, 171–175. [PubMed: 5124915]
- Olivo D, Caba M, Gonzalez-Lima F, Rodríguez-Landa JF, and Corona-Morales AA (2017). Metabolic activation of amygdala, lateral septum and accumbens circuits during food anticipatory behavior. *Behav. Brain Res* 316, 261–270. [PubMed: 27618763]
- Olton DS (1987). The radial arm maze as a tool in behavioral pharmacology. *Physiol. Behav* 40, 793–797. [PubMed: 3313453]
- Parfitt GM, Nguyen R, Bang JY, Aqrabawi AJ, Tran MM, Seo DK, Richards BA, and Kim JC (2017). Bidirectional control of anxiety-related behaviors in mice: role of inputs arising from the ventral Hippocampus to the lateral septum and medial prefrontal cortex. *Neuropsychopharmacology* 42, 1715–1728. [PubMed: 28294135]
- Petrovich GD, Canteras NS, and Swanson LW (2001). Combinatorial amygdalar inputs to hippocampal domains and hypothalamic behavior systems. *Brain Res. Brain Res. Rev* 38, 247–289. [PubMed: 11750934]
- Risold PY, and Swanson LW (1996). Structural evidence for functional domains in the rat hippocampus. *Science* 272, 1484–1486. [PubMed: 8633241]
- Ritter RC, Slusser PG, and Stone S (1981). Glucoreceptors controlling feeding and blood glucose: location in the hindbrain. *Science* 213, 451–452. [PubMed: 6264602]

- Rowland DC, Roudi Y, Moser MB, and Moser EI (2016). Ten years of grid cells. *Annu. Rev. Neurosci* 39, 19–40. [PubMed: 27023731]
- Suarez AN, Hsu TM, Liu CM, Noble EE, Cortella AM, Nakamoto EM, Hahn JD, De Lartigue G, and Kanoski SE (2018). Gut vagal sensory signaling regulates hippocampus function through multi-order pathways. *Nat. Commun* 9, 2181. [PubMed: 29872139]
- Suarez AN, Liu CM, Cortella AM, Noble EE, and Kanoski SE (2020). Ghrelin and orexin interact to increase meal size through a descending Hippocampus to hindbrain signaling pathway. *Biol. Psychiatry* 87, 1001–1011. [PubMed: 31836175]
- Swanson LW (2018). Brain maps 4.0-Structure of the rat brain: an open access atlas with global nervous system nomenclature ontology and flatmaps. *J. Comp. Neurol* 526, 935–943. [PubMed: 29277900]
- Swanson LW, and Cowan WM (1977). An autoradiographic study of the organization of the efferent connections of the hippocampal formation in the rat. *J. Comp. Neurol* 172, 49–84. [PubMed: 65364]
- Sweeney P, and Yang Y (2015). An excitatory ventral hippocampus to lateral septum circuit that suppresses feeding. *Nat. Commun* 6, 10188. [PubMed: 26666960]
- Terrill SJ, Jackson CM, Greene HE, Lilly N, Maske CB, Vallejo S, and Williams DL (2016). Role of lateral septum glucagon-like peptide 1 receptors in food intake. *Am. J. Physiol. Regul. Integr. Comp. Physiol* 311, R124–R132. [PubMed: 27194565]
- Terrill SJ, Subramanian KS, Lan R, Liu CM, Cortella AM, Noble EE, and Kanoski SE (2020). Nucleus accumbens melanin-concentrating hormone signaling promotes feeding in a sex-specific manner. *Neuropharmacology* 178, 108270. [PubMed: 32795460]
- Thompson RH, and Swanson LW (2010). Hypothesis-driven structural connectivity analysis supports network over hierarchical model of brain architecture. *Proc. Natl. Acad. Sci. USA* 107, 15235–15239. [PubMed: 20696892]
- Tingley D, McClain K, Kaya E, Carpenter J, and Buzsáki G (2021). A metabolic function of the hippocampal sharp wave-ripple. *Nature* 597, 82–86. [PubMed: 34381214]
- Trent NL, and Menard JL (2010). The ventral hippocampus and the lateral septum work in tandem to regulate rats' open-arm exploration in the elevated plus-maze. *Physiol. Behav* 101, 141–152. [PubMed: 20451539]
- Wang C, and Kotz CM (2002). Urocortin in the lateral septal area modulates feeding induced by orexin A in the lateral hypothalamus. *Am. J. Physiol. Regul. Integr. Comp. Physiol* 283, R358–R367. [PubMed: 12121849]
- Wirtshafter HS, and Wilson MA (2020). Title: differences in reward biased spatial representations in the lateral septum and hippocampus. *Elife* 9, e55252. [PubMed: 32452763]
- Yeates DCM, Leavitt D, Sujanthan S, Khan N, Alushaj D, Lee ACH, and Ito R (2022). Parallel ventral hippocampus-lateral septum pathways differentially regulate approach-avoidance conflict. *Nat. Commun* 13, 3349. [PubMed: 35688838]
- Zigman JM, Jones JE, Lee CE, Saper CB, and Elmquist JK (2006). Expression of ghrelin receptor mRNA in the rat and the mouse brain. *J. Comp. Neurol* 494, 528–548. [PubMed: 16320257]
- Zingg B, Chou XL, Zhang ZG, Mesik L, Liang F, Tao HW, and Zhang LI (2017). AAV-mediated anterograde transsynaptic tagging: mapping corticocollicular input-defined neural pathways for defense behaviors. *Neuron* 93, 33–47. [PubMed: 27989459]

**Highlights**

- Ventral hippocampus activity increases during memory retrieval for food location
- Ventral CA1-lateral septum circuitry encodes food- and water-based spatial memory
- This circuitry does not regulate spatial memory in an escape-based procedure
- Ventral CA1-lateral septum foraging circuitry targets the lateral hypothalamus

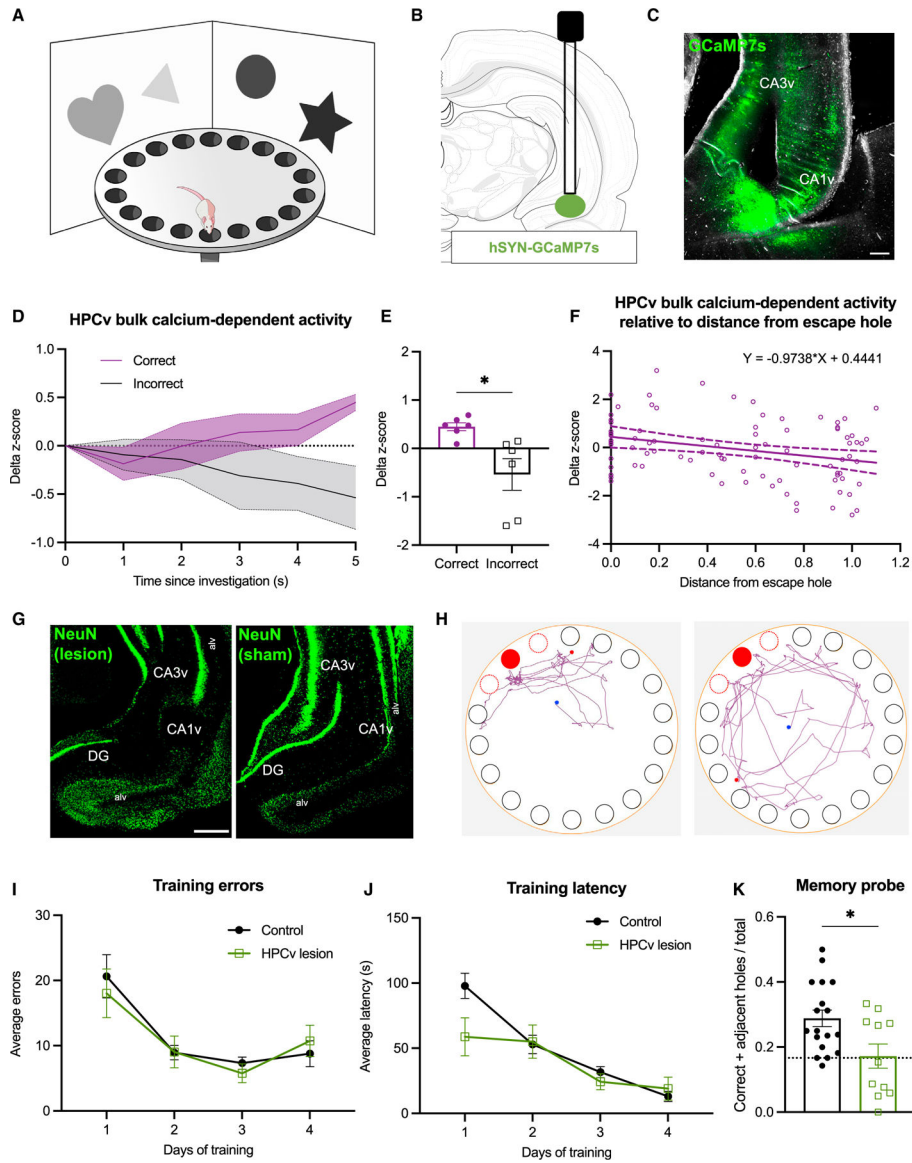


**Figure 1. Bilateral HPCv lesions impair spatial memory for food location**

(A) Spatial foraging task apparatus.

(B) Diagram of stereotaxic viral infusion (AAV-hSYN-GCaMP7s) and placement of optic fiber in the HPCv for bulk photometry recordings.

(C) Representative histology of GCaMP7s expression in HPCv neurons. Scale bar, 100  $\mu$ m.

(D) Variation in HPCv bulk calcium-dependent activity following a correct or incorrect investigation during a spatial food-seeking task (time  $\times$  investigation type,  $p < 0.05$ ).

(E) Delta Z score 5 s following a correct versus incorrect investigation during a spatial food-seeking task ( $p < 0.05$ ).

(F) Simple linear regression of delta Z score 5 s following investigation relative to distance of investigated hole from correct escape hole ( $p < 0.01$ ).

(G) Representative HPCv lesion histology with NeuN immunohistochemistry. Scale bar, 500  $\mu$ m.

(H) Left: representative navigation paths of a control animal preferentially investigating correct (filled red) and adjacent holes (outlined orange) during spatial foraging memory probe. Right: representative navigation path of HPCv lesioned animal during spatial foraging memory probe.

(I and J) Bilateral HPCv lesions did not impair learning of the spatial foraging task compared with controls, as measured by errors before locating correct hole during task training (I) and latency to locate correct hole during task training (J).

(K) Bilateral HPCv lesions impaired retention of the spatial foraging task, as measured by the ratio of investigation of correct plus adjacent holes over total investigated during the first minute of the task ( $p < 0.05$ ). Dotted line indicates chance performance level (0.1667).

For graphs (D), (E), and (F),  $n = 6$  (within-subjects). For graphs (I), (J), and (K), lesion  $n = 11$ , control  $n = 18$ . All values expressed as mean  $\pm$  SEM.

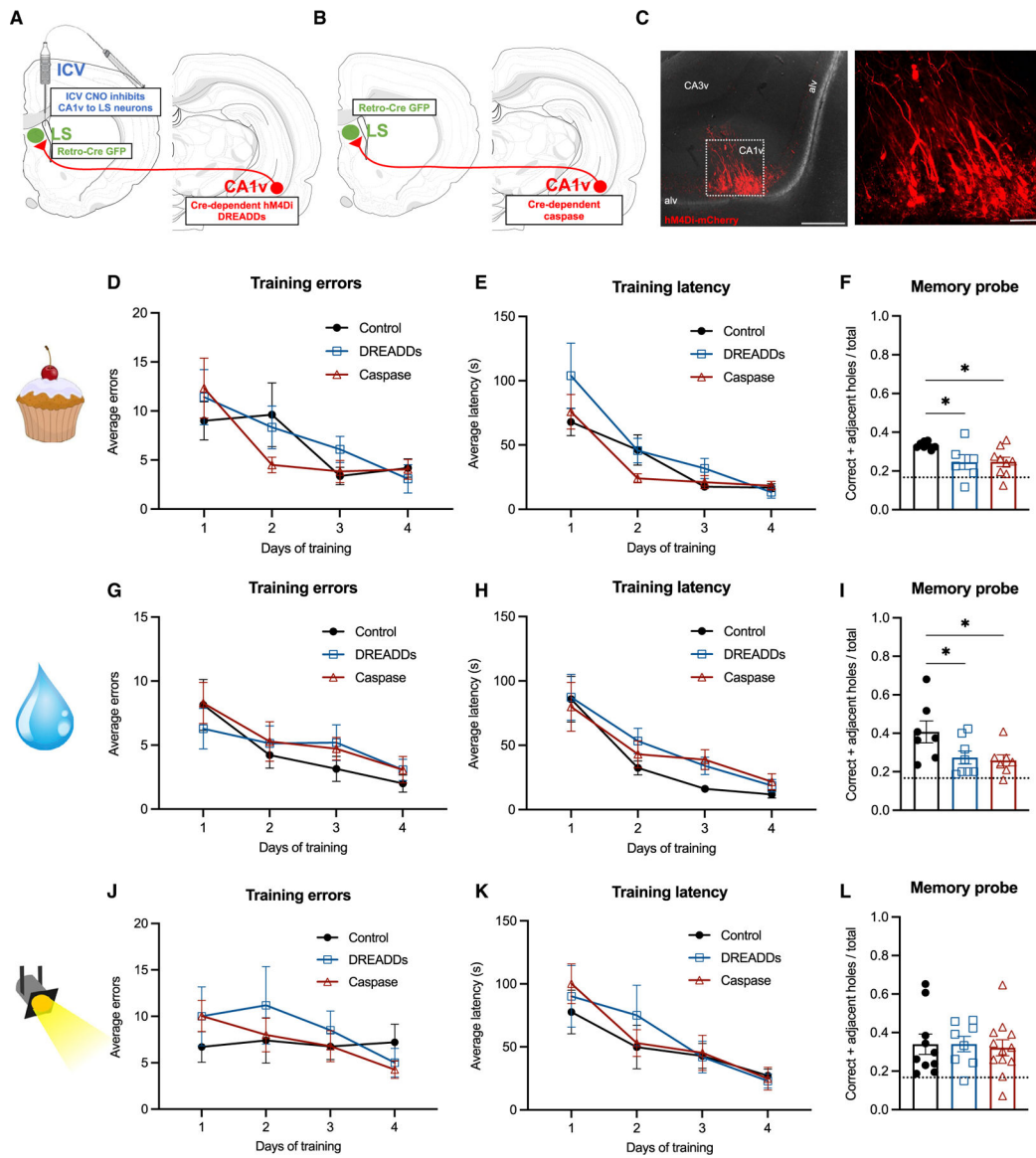


**Figure 2. Reversible and chronic CA1v-to-LS neural disconnection impairs spatial memory for food and water location but not for escape location**

(A) Diagram of dual viral approach using a Cre-dependent inhibitory DREADDs (AAV-hSyn-DIO-hM4D(GI)-mCherry) approach to reversibly disconnect CA1v-to-LS neural pathway (with CNO injected 1 h before memory probe).

(B) Diagram of dual viral approach using a Cre-dependent caspase (AAV1-Flex-taCasp3-TEVp) approach to chronically disconnect CA1v-to-LS neural pathway.

(C) Representative injection site in CA1v demonstrating LS-projecting neurons infected with inhibitory DREADDs, which simultaneously drives expression of a fluorescent mCherry transgene. Scale bars, 500  $\mu$ m (left) and 100  $\mu$ m (right).

(D and E) Neither reversible (DREADDs) nor chronic (caspase) disconnection of the CA1v-to-LS pathway impaired learning of the spatial food-seeking task compared with controls, as measured by errors before correct hole during task training (D) and latency to correct hole during task training (E).

(F) Both reversible and chronic disconnection of the CA1v-to-LS pathway impaired retention of the food location as measured by the ratio of investigation of correct plus adjacent holes over total investigations during entire 2 min of the task ( $p < 0.05$ ).

(G–I) Likewise, reversible (DREADDs) and chronic (caspase) disconnection of the CA1v-to-LS pathway did not impair learning of the spatial water-seeking task compared with controls, as measured by errors before correct hole during task training (G) and latency to correct hole during task training (H), but impaired memory retention of the water location during the probe (I).

(J and K) In contrast, disconnection of the CA1v-to-LS pathway either reversibly (DREADDs) or chronically (caspase) did not impair performance on the spatial escape task. There were no differences in learning as measured by errors before correct hole during task training (J) and latency to correct hole during task training (K).

(L) Unlike the spatial foraging task, retention of the spatial escape task was not impaired by reversible or chronic disconnection of the CA1v-to-LS pathway. For graphs (E), (F), and (G) (CA1v-to-LS disconnect cohort 1), DREADDs  $n = 6$ , caspase  $n = 10$ , control  $n = 8$ . For graphs (H), (I), and (J) (CA1v-to-LS disconnect cohort 3), DREADDs  $n = 8$ , caspase  $n = 8$ , control  $n = 7$ . For graphs (K), (L), and (M) (CA1v-to-LS disconnect cohort 2), DREADDs  $n = 8$ , caspase  $n = 12$ , control  $n = 10$ . Dotted line indicates chance performance level (0.1667). All values expressed as mean  $\pm$  SEM.

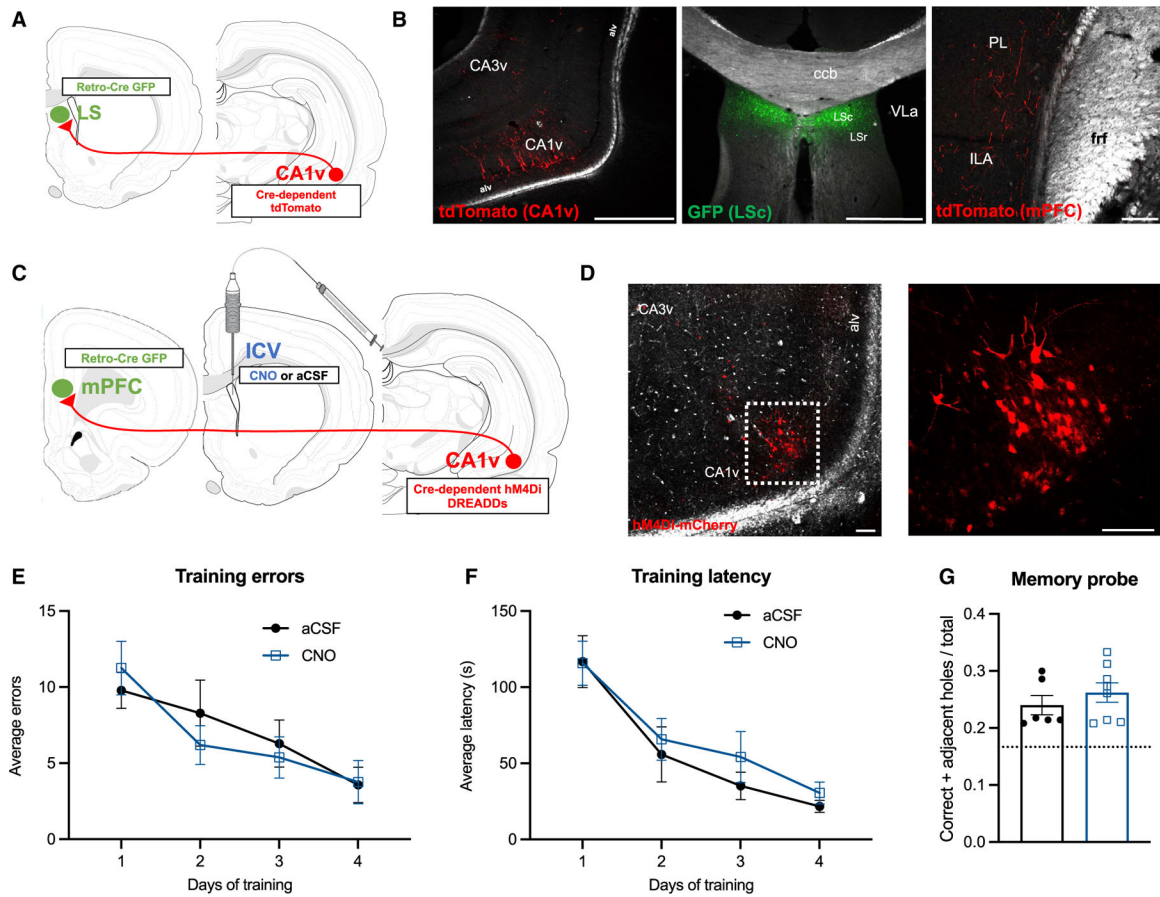


**Figure 3. CA1v to mPFC projections do not contribute to appetitive spatial memory**

(A) Diagram of dual viral approach to identify collateral targets of the CA1v-to-LS neural pathway.

(B) Left: representative CA1v injection site from collateral identification approach. Scale bar, 500  $\mu$ m. Middle: representative LS injection site from collateral identification approach in relation to the caudal (LSc) and rostral (LSr) subregions, the corpus callosum body (ccb), and lateral ventricle (VL<sub>a</sub>). Scale bar, 500  $\mu$ m. Right: representative image collateral axons of the CA1v-to-LS pathway located in the prelimbic (PL) and infralimbic (ILA) areas of the mPFC. Scale bar, 50  $\mu$ m.

(C) Diagram of dual viral approach using Cre-dependent inhibitory DREADDs (AAV-hSyn-DIO-hM4D(GI)-mCherry) to acutely disconnect the CA1v-to-mPFC neural pathway (with CNO or aCSF injected 1 h before memory probe).

(D) Representative injection site in CA1v demonstrating mPFC-projecting neurons infected with inhibitory DREADDs, which simultaneously drives expression of a fluorescent mCherry transgene. Scale bars, 100  $\mu$ m.

(E and F) Disconnection of the CA1v-to-mPFC neural pathway did not influence learning of the spatial foraging task compared with controls, as measured by errors before correct hole during training (E) and latency to correct hole during training (F).

(G) Disconnection of the CA1v-to-mPFC pathway did not influence retention of the spatial foraging task in the memory probe.

For graphs (E), (F), and (G), aCSF n = 6, CNO n = 8. Dotted line indicates chance performance level (0.1667). All values expressed as mean  $\pm$  SEM.

Author Manuscript

Author Manuscript

Author Manuscript

Author Manuscript

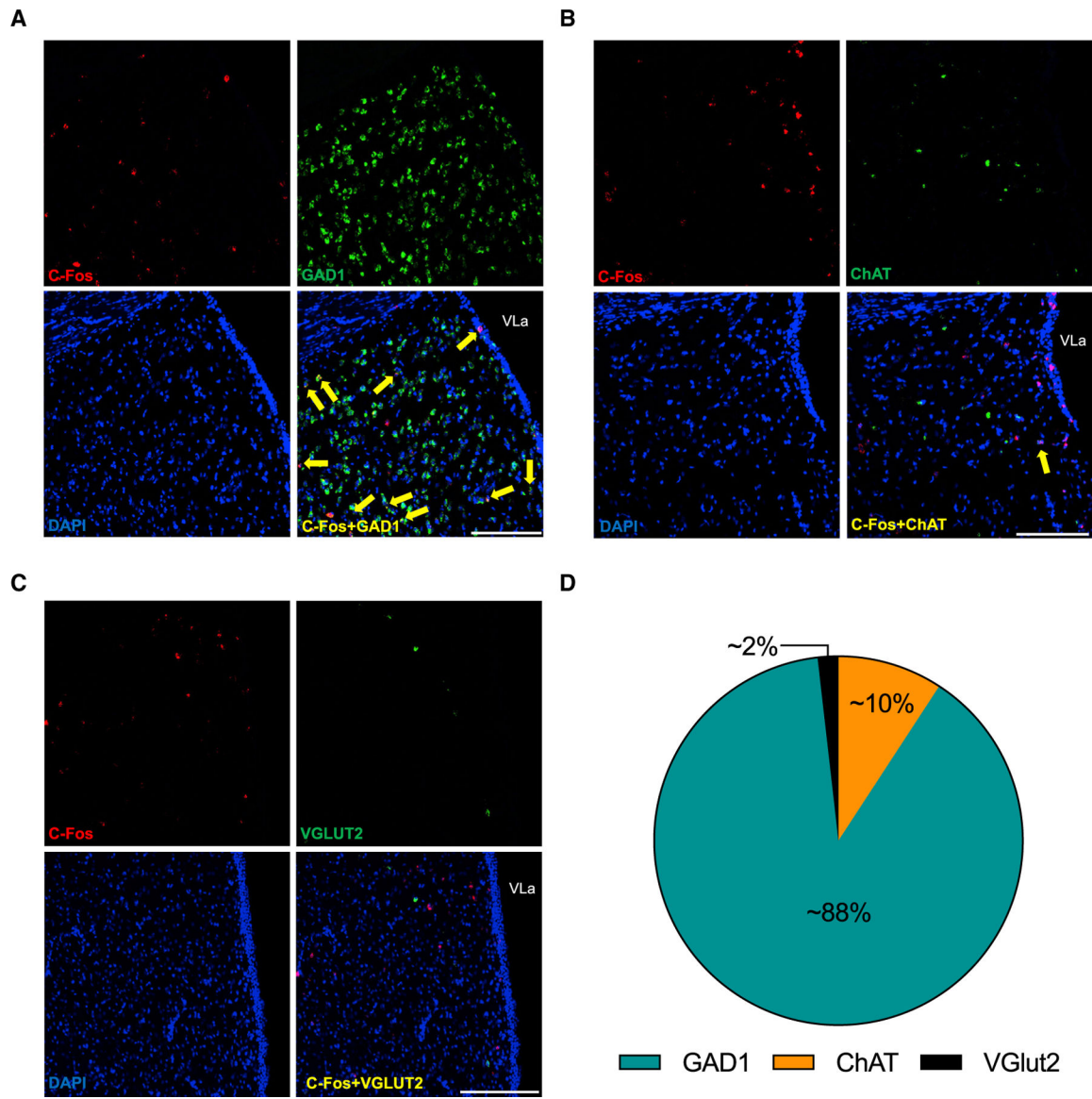


**Figure 4. LS neurons activated during food-seeking memory probe are predominantly GABAergic**

(A–C) c-Fos and ChAT colocalization was observed in ~2% of LS neurons (A; scale bar, 500  $\mu$ m), c-Fos and GAD1 colocalization was observed in ~88% of LS neurons (B; scale bar, 500  $\mu$ m), and c-Fos and VGLUT2 colocalization was observed in ~10% of LS neurons (C; scale bar, 500  $\mu$ m) following the spatial memory probe test (for food reinforcement).

(D) Percentage of c-Fos<sup>+</sup> LS neurons expressing GABAergic, cholinergic and glutamatergic markers. Quantification from DREADDs vehicle group, n = 3.

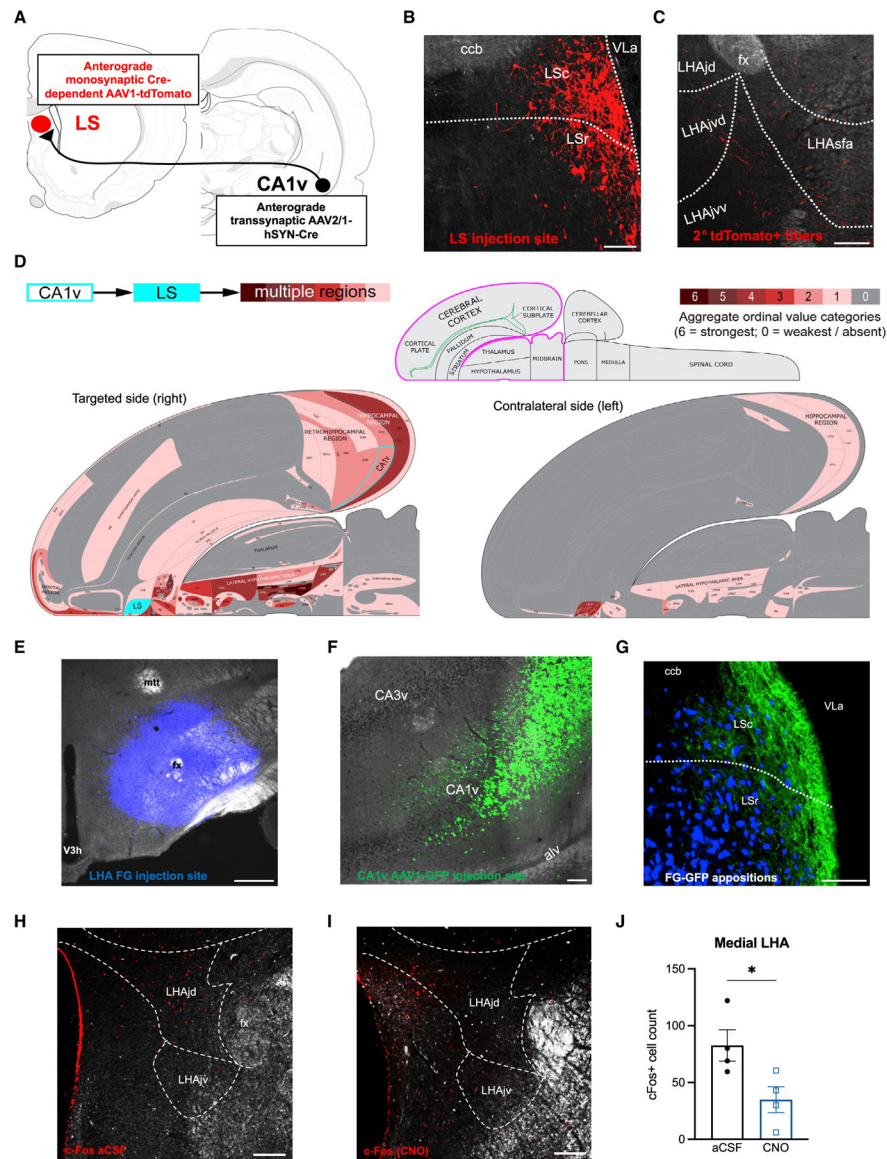


### Figure 5. Identification of second-order neural projections downstream of CA1v-to-LS projections

(A) Diagram of dual viral approach to identify brain regions that are second-order ( $2^{\circ}$ ) targets of the CA1v-to-LS neural pathway.

(B) Representative LS injection site from second-order identification approach in relation to the caudal (LSc) and rostral (LSr) subregions, the corpus callosum body (ccb), and lateral ventricle (VL<sub>a</sub>). Scale bar, 100  $\mu$ m.

(C) Representative image of second-order fibers of the CA1v-to-LS pathway within the juxtadorsomedial (jd), juxtaventromedial dorsal (jvd), juxtaventromedial ventral (jvv), and subfornical anterior (sfa) subregions of the LHA. Scale bar, 200  $\mu$ m.

(D) Summary of the projection targets of LS neurons that receive input from CA1v (for expanded information see Table S1). The outputs of the right side of LS neurons receiving CA1v input are represented at the macroscale (gray matter region resolution) on a partial flatmap representation of the rat forebrain, adapted from Hahn et al. (2021). Connection

weights are represented by block colors for each region following an ordinal scale ranging from weakest (0 = very weak or absent) to strongest (6 = strong), as there were no 7 (very strong) values. The lower panels represent one side of the brain with the part represented in the upper diagram outlined in magenta.

(E–G) The COIN approach for further confirmation of second-order tracing strategy is depicted with FG injection site in the LHA (E; scale bar, 500  $\mu\text{m}$ ), representative AAV1-GFP injection site in the CA1v (F; scale bar, 100  $\mu\text{m}$ ), and FG-GFP appositions in the LS (G; scale bar, 100  $\mu\text{m}$ ).

(H) Representative histology of c-Fos expression in the medial LHA (LHAjd and LHAjv) following i.c.v. infusion of aCSF. Scale bar, 200  $\mu\text{m}$ .

(I) Representative histology of c-Fos expression in the medial LHA (LHAjd and LHAjv) following i.c.v. infusion of CNO to inhibit LS-projecting CA1v neurons, Scale bar, 200  $\mu\text{m}$ .

(J) Counts of c-Fos-positive cells in the medial LHA (LHAjd and LHAjv) are reduced with i.c.v. administration of CNO ( $p < 0.05$ ). aCSF  $n = 4$  and CNO  $n = 4$ . Values expressed as mean  $\pm$  SEM.

## KEY RESOURCES TABLE

REAGENT or RESOURCE	SOURCE	IDENTIFIER
Antibodies		
Chicken anti-GFP	Abcam	Cat. no. ab13970; RRID:AB_300798
Donkey anti-chicken AF488	Jackson Immunoresearch	RRID: AB_2340375
Donkey anti-rabbit AF488	Jackson Immunoresearch	RRID: AB_2340619
Donkey anti-rabbit Cy3	Jackson Immunoresearch	RRID: AB_2307443
Rabbit anti-MCH	Phoenix Pharmaceuticals	Cat. no. H_070_47; RRID:AB_10013632
Rabbit anti-NeuN	Abcam	Cat. no. Ab177487; RRID:AB_2532109
Rabbit anti-RFP	Rockland	RRID: AB_2209751
Rabbit anti-orexin	EMD Millipore	Cat. no. AB3704; RRID:AB_91545
Bacterial and virus strains		
AAV1-CAG-Flex-tdTomato-WPRE-bGH	UPenn Vector Core	N/A
AAV2-Flex-hM4i-mCherry	Addgene	Cat. no. 44362-AAV2
AAV1-Flex-taCasp3-TEVp	UNC Vector Core	N/A
AAV1-hSyn-Cre-WPRE-hGH	UPenn Vector Core	N/A
AAV1-hSyn-eGFP-WPRE-bGH	Vector BioLabs	Cat. no. VB4870
AAV2[retro]-hSYN1-EGFP-2A-iCre-WPRE	Vector BioLabs	Cat. no. VB4855
AAV9-hSyn-GCaMP7s-WPRE	Addgene	Cat. no. 104487-AAV9
Chemicals, peptides, and recombinant proteins		
Clozapine-N-oxide	RTI International	N/A
NMDA	Sigma	M3262
Fluorogold	Fluorochrome	N/A
Deposited data		
Original data	This paper	OSF: <a href="https://osf.io/rb2w8/">https://osf.io/rb2w8/</a>
Experimental models: Organisms/strains		
Sprague Dawley rat	Envigo	RRID:RGD_737903
Oligonucleotides		
c-Fos	ACD	Cat. no. 403591
ChAT	ACD	Cat. no. 430111
GAD1	ACD	Cat. no. 316401
vGLUT2	ACD	Cat. no. 317011
Software and algorithms		
AnyMaze Behavior Tracking Software	Stoelting	N/A
MatLAB	MathWorks	N/A

REAGENT or RESOURCE	SOURCE	IDENTIFIER
Statistica	StatSoft	N/A
Axiome C	Hahn et al., 2021	N/A
Other		
Original MatLab code	This paper	OSF: <a href="https://osf.io/rb2w8/">https://osf.io/rb2w8/</a>

Author Manuscript

Author Manuscript

Author Manuscript

Author Manuscript